

LEAST SQUARE BASED ARTIFICIAL COMPRESSIBILITY METHOD

By

MIHIR CHATTERJEE

(Enrolment No. ENGG01200603002)

Bhabha Atomic Research Centre, Mumbai

*A dissertation submitted to the
Board of Studies in Engineering Sciences
In partial fulfillment of requirements
For the Degree of*

MASTER OF SCIENCE (Engineering)

of

HOMI BHABHA NATIONAL INSTITUTE



August, 2009

Homi Bhabha National Institute

Recommendations of the Thesis Examining Committee

As members of the Thesis examining Committee, we recommend that the dissertation prepared by Sri Mihir Chatterjee entitled “Least Square Based Artificial Compressibility Method” be accepted as fulfilling the dissertation requirement for the Degree of Master of Science (Engineering).

	Name	Signature
Member-1	Prof. R. K. Singh	
Member-2	Prof. J. Mandal	
Examiner-1	Prof. A. Sharma	
Examiner-2	Dr. N. K. Maheshwari	
Co-guide	Sri. A. K. Mahendra	
Guide / Convener	Prof. P. K. Vijayan	
Chairman	Prof. L. M. Gantayet	

Date: August 25, 2009

Place: BARC, Mumbai

DECLARATION

I, hereby declare that the investigation presented in the thesis has been carried out by me. The work is original and has not been submitted earlier as a whole or in part for a degree / diploma at this or any other Institution / University.

(Mihir Chatterjee)

DEDICATIONS

To my parents who's blessing is always with me, my wife Nupur who always stands beside me and my son Nirmalya who's innocence is inspiration to me.

ACKNOWLEDGEMENTS

While sitting to write about the acknowledgements, I'm overwhelmed by the number of people I am indebted to by one way or other. First and foremost I should name Prof. S. M. Deshpande whose meshless LSKUM method has inspired me for the present work. The wonderful memory of long discussions with a personality like him itself is a treasure for me. Next I should express my sincere gratitude towards my respected guide, Professor P. K. Vijayan for the interest he has taken in my work and for the help and guidance he has provided me, by spending his precious time, throughout the present spell of work. I am greatly indebted to my co-guide Shri A.K. Mahendra for his constant encouragement and timely help for my work without which it would have been extremely difficult for me to complete this work. His constant endeavor for attaining perfection is truly one of the greatest learning during the course. I'm indebted to Prof. J. C. Mandal from IIT Bombay for his invaluable suggestions during the mid term review. My colleague Shri Vinay was always ready to lend a helping hand, be it a required mesh or be it some related technical paper. Thank you very much Vinay. I still remember the day when I visited Shri Santa Kumar Lahiri's residence a day before our FEM examination, and how meticulously Lahiri'da taught me the subject. Thanks Lahiri'da. Finally I would like to thank my section head Shri A. Sanyal and my division head Shri G. Gouthaman for their moral support during the entire work period, which led me to work in the right direction.

CONTENTS

		Page No.
SYNOPSIS		vii
LIST OF FIGURES		viii
LIST OF TABLES		x
NOMENCLATURE		xi
CHAPTER 1	Introduction	1
	1.0 Objective of the current work	1
	1.1 Grid generation and meshless method	3
	1.2 Discretization and meshless method	5
	1.3 Various meshless methods and their advantages	6
	1.4 Organization of thesis	7
CHAPTER 2	Incompressible Flow Simulation using Artificial Compressibility Method (ACM)	8
	2.0 Introduction	8
	2.1 Literature survey on artificial compressibility method	11
	2.2 Significance of artificial compressibility parameter δ	15
	2.3 Values of artificial compressibility parameter δ	17
	2.4 Governing equations of ACM in flux form	22
	2.5 Summary	23

CHAPTER 3	Meshless Code Development	24
	3.0 Literature survey on meshless methods	24
	3.1 Least square based discretisation	27
	3.2 Incorporation of upwind scheme	28
	3.3 Detailed features of the code	31
	3.4 Code details	33
	3.5 Schematic of code	35
	3.6 Summary	36
CHAPTER 4	Code Validation	37
	4.0 Introduction	37
	4.1 Fully developed flow between two parallel plates	37
	4.2 Isothermal laminar flow	40
	4.2.1 External flow over a flat plate (Blasius Solution)	40
	4.2.2 Flow inside a lid driven cavity	43
	4.3 Flow past a circular cylinder	48
	4.4 Flow over a backward facing step	55
	4.5 Laminar axisymmetric sudden expansion flow	62
	4.6 Condition number analysis	66
	4.7 Summary	68
CHAPTER 5	Conclusions and Future work	70
	5.0 Conclusions	70
	5.1 Future work	72
	Appendix A	73
	Appendix B	75
	REFERENCES	79

SYNOPSIS

The objective of the current research is to develop a meshless method based on least squares to solve incompressible Navier-Stokes equations. The meshless method based on least squares depends on arbitrary distribution of points called cloud of points and it requires connectivity and neighbourhood information for every point in the cloud. The present study is aimed at applying an upwind differencing scheme in conjunction with pseudocompressibility method in mesh less framework. Recently meshless methods for many compressible flow algorithms have gained popularity. All meshless numerical methods share a common feature that no mesh is needed and the solver is capable of operating on an arbitrary distribution of points. For a multibody configuration, clouds of points are generated around every part or component of the body and these clouds around components are then merged to obtain a distribution of points around it. For carrying out numerical simulation of Navier-Stokes equations for complex multibody configuration, generation of a suitable grid becomes the most difficult job. The pseudocompressibility method was first introduced by Chorin for solving complex incompressible flow problems. In this formulation, a time derivative of pressure is added to the continuity equation. Together with the momentum equations, these form a hyperbolic system of equations, which can be marched in pseudo-time to a steady state solution. In the present work an attempt has been made to use the artificial compressibility method with meshless least square based discretisation for solving incompressible Navier-Stokes equations. The advantage of this least square based meshless pseudocompressibility method is that it can be used to solve incompressible flow problem around complex geometry where the task of grid generation can be simplified by generation of cloud of points around the body and their connectivity information.

LIST OF FIGURES

Fig No.	Title of figure	Page No.
3.1	Typical connectivity around point P_o	27
3.2	Stencil splitting for upwinding	29
3.3	Schematic of the code developed	36
4.1a	Computational domain	36
4.1b	Grid for flow between parallel plates	36
4.2	Reynolds number contours and residue plot for flow between parallel plates	40
4.3	External flow over a flat plate	41
4.4	Grid used for Blasius problem	41
4.5	Reynolds number contour	42
4.6a	Present and Blasius solution for flow over flat plate	43
4.6b	Residue plot for flow over flat plate	43
4.7	Lid-driven cavity problem: nodes with boundary conditions	44
4.8	Predicted velocity distribution for the lid driven cavity problem at $Re=100$.	45
4.9	Predicted velocity distribution for the lid driven cavity problem at $Re=400$	46
4.10	Predicted stream line plot and velocity distribution for the lid driven cavity problem at $Re=1000$	47
4.11	Configuration of flow past a circular cylinder	48
4.12	Composite grid	49
4.13	Detailed grid structure	49
4.14a	Reynolds number contour, streamline and residual plot for flow past circular cylinder at Reynolds number=20	51

4.14b	Reynolds number contour, streamline and residue plot for flow past circular cylinder at Reynolds number=30	52
4.14c	Reynolds number contour, streamline and residue plot for flow past circular cylinder at Reynolds number=40	53
4.15	Characteristic parameters of the cylinder's wake	54
4.16	Outline of the backward facing step problem	56
4.17	Grid used for computation of flow over backward facing step	57
4.18	Streamline plot for flow over a backward facing step at different Reynolds number	59
4.19	Variation of x_1 , x_2 and x_3 with Reynolds number	60
4.20	Velocity profiles for various downstream locations for $Re=100$; Top figure Armaly et.al (1983), middle figure Erturk (2008), bottom figure present	61
4.21	Geometry and boundary conditions used for sudden expansion flow problem	63
4.22	Streamline plots for sudden expansion problem for different Reynolds number	64
4.23	Comparison of Dependence of reattachment length on Reynolds number	65
4.24	Condition number contours for flow simulation using meshless ACM based solver over different geometries	68

LIST OF TABLES

Table No.	Title of Table	Page No.
4.1	Comparison of length of re-circulating region (L_{sep}), separation angle (θ_{sep}) and drag coefficient (C_d) for $Re= 20$ and 40	55
4.2	Values of condition number and artificial compressibility parameter	67

NOMENCLATURE

c	Sound speed, m/s
C	Arbitrary constant, dimensionless
C_d	Drag Coefficient, dimensionless
d	Diameter of pipe, m
Δd	Distance between a point and it's neighbor, m
e	Internal energy per unit mass, J/kg
E	Square of error in Taylor series expansion
f_x	Space derivative with respect to x
f_y	Space derivative with respect to y
$f_{x_o}^{(1)}$	First order accurate space derivative of f with respect to x at point o
$f_{x_o}^{(2)}$	Second order accurate space derivative of f with respect to x at point o
$f_{y_o}^{(1)}$	First order accurate space derivative with respect to y at point o
$f_{y_o}^{(2)}$	Second order accurate space derivative of f with respect to y at point o
$\{f_{x_o}\}_{N_1(P_o)}$	X derivative of scalar f at point P_o evaluated using sub stencil set $N_1(P_o)$
$\{f_{x_o}\}_{N_2(P_o)}$	X derivative of scalar f at point P_o evaluated using sub stencil set $N_2(P_o)$
$\{f_{y_o}\}_{N_3(P_o)}$	Y derivative of scalar f at point P_o evaluated using sub stencil set $N_3(P_o)$
$\{f_{y_o}\}_{N_4(P_o)}$	Y derivative of scalar f at point P_o evaluated using sub stencil set $N_4(P_o)$
F_D	Drag force, N
h	Height of channel, m

Δh	Mesh width, m
k_1, k_2	Real positive constants that depends on Reynolds number
L	Length scale, m
L_r	The reattachment length, m
Ma	Mach Number, dimensionless
p	Physical pressure, Pa
p'	Pressure per unit density
P_o	Point o
r	Radius of cylinder, m
R	Specific universal gas constant, $JK^{-1}mol^{-1}$
Re	Reynolds number, dimensionless
s	Step Height of backward facing step, m
t	Time, s
Δt	Time step, s
T	Temperature in absolute scale, K
u	x component of velocity, m/sec
$u_{g,c}$	Horizontal velocity component along the vertical mid plane of the cavity, m/s
u_∞	Free stream velocity, m/s
U	State vector
U_{ref}	Reference velocity, m/s
v	y component of velocity, m/s
$v_{g,c}$	Vertical velocity component along the horizontal mid plane of the cavity, m/s
w	Z component of velocity, m/s
w_i	Weight factor
x_δ	Half distance between two walls for simple channel flow, m
X_{ref}	Reference length, L
x_1	Length of primary circulation zone behind backward facing step, m

x_2	Distance of starting point of secondary circulation zone from backward facing step, m
x_3	Distance of end point of secondary circulation zone from backward facing step, m
Δx_i	Distance in x direction between a point and its neighbor, m
Δy_i	Distance in y direction between a point and its neighbor, m
y	Distance in y direction, m
z	Distance in z direction, m
$\ A\ $	Norm of matrix A

Greek Symbols

δ	Artificial compressibility parameter, Pa-m ³ /kg
δ_{opt}	Optimal value of δ , Pa-m ³ /kg
ε_s	Small value introduced to avoid ill conditioning near stagnation points
γ	Ratio of specific heats
κ	Condition number, product of norm of a matrix and norm of inverse of the matrix
λ	Eigenvalues of a matrix
μ	Viscosity, kg/m-s
ν	Kinematic viscosity, m ² s ⁻¹
θ_{sep}	Separation angle, degree
ρ	Density, kg/m ³
σ	Singular value of a matrix
τ	Pseudo time scale, sec
τ_{ij}	Components of shear stress on the i th plane in j th direction
ω	Vorticity, s ⁻¹
\aleph	Value of a field variable
\Re	Residual

CHAPTER 1

Introduction

1.0 Objective of the current work

The objective of the current work is to find a suitable method of solution for the incompressible Navier-Stokes equations using meshless least square based method for flow past complex geometries. The present study is aimed at applying an upwind differencing scheme in conjunction with pseudocompressibility method in mesh less framework. The pseudocompressibility method was first introduced by Chorin (1968) and has been used extensively with much success by Kwak et al. (1986) for solving complex incompressible flow problems. In this formulation, a time derivative of pressure is added to the continuity equation. Together with the inviscid momentum equations, these form a hyperbolic system of equations, which can be marched in pseudo-time to a steady state solution. The method can also be extended to solve time dependent problems (Merkle et al. (1987)) by using sub iterations in pseudotime at every physical time step to ensure divergence-free velocity field. If only steady state solution to a problem is required, the pseudocompressibility method can be a very efficient formulation because it does not require that divergence-free velocity field be obtained at each iteration but only as the solution converges. The addition of the time derivative of pressure to the continuity equation creates a hyperbolic system of equations complete with artificial pressure waves of finite speed. When the solution converges to a steady state, a divergence free flow field is obtained. Hence many of the well-developed compressible flow algorithms can be utilized for this method.

Meshless methods, as promising numerical methods, have been developed and made a remarkable progress in the past few decades. It provided alternative and innovative ways to solve various kinds of problems in many fields.

As its name implies, there is no conventional grid used in the meshless method. This attractive feature has drawn many attentions from the scientists, engineers and researchers. Without the use of the conventional grid, meshless methods not only avoid mesh-related difficulties that often encountered in the conventional mesh-related method such as FEM, but also facilitate adaptive analyses. Refinement and coarsening process in the meshless adaptive analysis can be performed simply by inserting or removing node conveniently. Though the computational effort involved in such calculations is considerably more compared to the routine structured mesh calculations, the ever-increasing speed of the computers has made these computations more realistic. Grid-free methods also address the question of computation of flow past complex configurations. To approximate derivatives at any given node, all these methods require, is the information at a cloud of grid points around that node.

Meshless methods eliminate some or all of the traditional mesh-based view of the computational domain and rely on a particle view of the field problem. Meshless (or 'meshfree' as this is also used) methods seem attractive as alternative to FEM for the general engineering community, which consider the process of generating finite element meshes as more difficult and expensive than the remainder of analysis process. Recently meshless methods for many compressible flow algorithms have gained popularity (Mahendra (2003)). All meshless numerical methods share a common feature that no mesh is needed and the solver is capable of operating on an arbitrary distribution of points. For carrying out numerical simulation of Navier-Stokes equations for complex multibody configuration, generation of a suitable grid becomes the most difficult job. In meshless methods this problem is addressed by obtaining arbitrary distribution of grid points around the multibody configuration (meshless method utilize connectivity set) using any method of grid generation (structured, unstructured, prismatic, Cartesian, chimera, hybrid etc.). The principal problem in any meshless method is to determine approximations to space derivatives in x and y direction at any node P_o using data at neighbouring points. The node P_o is surrounded by points distributed arbitrarily (termed as cloud of points). We define

the set of points at the neighbourhood as the connectivity (also called stencil). The distribution of points can be obtained by many techniques. The connectivity or the set of neighbours once obtained is used to compute the discrete approximations to the space derivatives at the point P_o using least squares. These in turn are used in the update formulae to obtain the solution at the next time level. In the present work least square based meshless method is used to solve incompressible Navier Stokes equations using pseudocompressibility method.

1.1 Grid generation and meshless method

Mesh generation is a very important part of any computational fluid dynamics solution and it can be very time consuming task for the analyst. In traditional grid based method like finite element method the entire domain has to be meshed properly with triangular or quadrilateral elements. Also there should not be any overlapping and gaps between the elements. The connectivity information among all the elements has to be computed during mesh generation and the solver requires this information during simulation. The task may become even more tedious and computationally intensive for complex multibody configuration. In the multiblock approach for grid generation the computational domain is composed of several blocks. The grid lines at the block interfaces are either continuous (composite grids) or discontinuous (patched). Multiblock approach for complex geometries becomes very tedious, as the user has to define large number of blocks of different orientation and sizes and their interfaces. Difficulties associated with multiblock approach led to the development of more flexible method called chimera processing. In this method the body fitted grids are generated for each component of a multibody configuration and the grids are allowed to overlap. Difficulty in this approach is in transferring information between regions and maintenance of conservation in the overlapped regions. The idea of making grids structured near the boundary and unstructured elsewhere to resolve the viscous flows led to the development of hybrid grids. Hybrid grids consisting of triangles and quadrilaterals in two-

dimension and tetrahedral and prisms in three-dimension provides the advantages of both structured and unstructured meshes. Ideally this mesh generation job can be fully automated but generally done by semi-automatic preprocessor packages that require the user to define zones of meshing, type of mesh elements (particularly near boundary) to be generated and different parameters like mesh clustering. Triangulation is the most flexible way to create mesh elements and therefore used more frequently and it is also suitable for modeling complex geometry.

Since meshless methods were born with the objective of eliminating part of the difficulties associated with reliance on a mesh to construct the approximation in a finite element methodology, the advantages and disadvantages of these methods are compared generally in the literature within the framework of FEM. Nguyen (2008) listed some major advantages of meshless methods are (i) h -adaptivity is simpler to incorporate in meshless methods than in mesh-based methods, (ii) problems with moving discontinuities such as crack propagation, shear bands and phase transformation can be treated with ease, (iii) large deformation can be handled more robustly, (iv) higher-order continuous shape functions, (v) non-local interpolation character and (vi) no mesh alignment sensitivity. Beside these advantages, meshless methods are not without disadvantages. The meshless methods shape functions are rational functions, which requires high-order integration scheme to be correctly computed. The treatment of essential boundary conditions is not as straightforward as in mesh-based methods since the meshless methods shape functions are not interpolants. They do not satisfy the Kronecker delta property. In general, the computational cost of meshless methods is higher than one of FEM.

In meshless method the computation domain is represented by a set of arbitrary distributed nodes, as there is no need to use meshes or elements for interpolation of field points. These methods are a group of techniques useful for solving partial differential equations on irregular grids. Though this group of

methods originated from works in the field of finite element methods, they can treat an irregular distribution of points and require no costly mesh generation. In meshless methods for a multibody configuration, clouds of points are generated around every part or component of the body and these clouds around components are then merged to obtain a distribution of points around the geometry. The nodes are generated by using simple grid generation methods that are easily available for both two and three dimensions. The significance of the meshless method is that the human intervention in the process of node generation is minimum and the process can be almost fully automated. The node generation also can be done in a fully adaptive manner and thus the total time required for mesh generation can be reduced significantly. In addition, since meshless methods use arbitrary placements of points, the solution and its derivatives may be found directly where they are needed. On the other hand, meshless input data contain much less information compared with the grid or mesh structures required by the traditional finite difference / finite element methods. The input data generation procedure for meshless codes are called 'node generation' which can be obtained by one or many simple pre-processors. All that is required for meshless node generation is a small portion of the preprocessor to generate triangular elements and only the nodes of those elements are retained while the elements are discarded. The variety of problems that are now being addressed by the meshless methods continues to expand and the quality of the results obtained demonstrates the effectiveness of many of the methods currently available (Yagawa, (2002)).

1.2 Discretization and meshless method

In computational fluid dynamics we discretize the governing differential equations based on discretized domains and a set of discrete simultaneous system of equations can be formulated from the original governing equations. These simultaneous equations are obtained based on four basic principles. The first is based on the principle of virtual work and the second is based on residual methods. Traditional grid based method of finite element method (FEM) is based

on these principles. The third discretization principle is based on the Taylor series, which has laid to the foundation of finite difference method (FDM). The fourth principle is based on the control of conservation laws in each finite volume in the domain. The finite volume method (FVM) was established following this approach. The first and the second principles are generally used predominantly for problems involving solids and structures while the third and fourth principles are routinely used more for fluid flow and heat transfer simulations. Most meshless method based on the first two principles are termed as weak form, and that based on the third principle is called strong form of implementation (Liu, (2003))

1.3 Various meshless methods and their advantages

Various methods belonging to this family of meshless methods include, Smooth Particle Hydrodynamics (SPH) methods by Lucy et. al. (1977) and Gingold and Monaghan, finite point method by Liszka and Orskisz (1980), Least Square Kinetic Upwinding Method (LSKUM) by Deshpande et. al. (1994), Diffuse Element Method (DEM) by Nayroles et al. (1992), Element Free Galerkin Method (EFG) by Belytschko et. al. (1994), Reproducing Kernel Particle Method (RKPM) and Moving Least Square Reproducing Kernel Method (MLSRKM) by Liu et. al. (1995), h (spatial partition)- p (degree of polynomial)-Clouds by Duarte and Oden (1996), Point Interpolation Method (PIM) by Liu and Gu (1999), Meshless Local Petrov-Galerkin Method (MLPG) by Atluri and Zhu (1998) and Atluri and Shen (2002). The main advantages of using meshless methods can be summarized as follows

- The bottleneck of node generation for complex geometry can be bypassed
- Any preprocessor available can be used for node generation for meshless methods
- The data structure of the node information required by the meshless method is simple

- The node generation also can be done in a fully adaptive manner
- The formulation is similar for two-dimension and three-dimensional problems
- It does not involve numerical integration
- Ease of coding
- Cost effectiveness due to man-power reduction involved for the meshing

1.3 Organization of Thesis

This Thesis is organized in the following way. Chapter 2 contains General introduction about Artificial Compressibility Method (ACM). Details about different previous work in ACM have been included in this chapter. The mathematical model developed for meshless ACM has been described in chapter 3. A few benchmark test problems have been solved using the code developed are given in chapter 4. Chapter 5 describes detailed features of the code, steps followed by the code, conclusion and further work. This is followed by appendices A, B and references.

CHAPTER 2

Incompressible Flow Simulation using Artificial Compressibility Method

2.0 Introduction

In this work an algorithm is developed for simulating incompressible steady flow on two-dimensional unstructured meshes. The Navier-Stokes equations are briefly reviewed as the basic governing equation for fluid flow. Using this set of equations, in the limit of incompressible flow, the problem of imposing the time independent continuity equation on the momentum equations arises. This difficulty can be removed by employing the artificial compressibility approach. This approach modifies the continuity equation by adding a pseudo pressure time derivative. This modification makes the set of equations well conditioned for numerical solution. If the set of modified equations is used for the solution of the steady state problems, the added pressure derivative tends to zero.

The two-dimensional continuity and momentum equation for any generalized flow field (assuming no body forces) can be expressed as,

$$\frac{\partial \rho}{\partial t} + \frac{\partial}{\partial x}(\rho u) + \frac{\partial}{\partial y}(\rho v) = 0 \quad (2.1)$$

$$\frac{\partial}{\partial t}(\rho u) + \frac{\partial}{\partial x}(\rho + \rho uu) + \frac{\partial}{\partial y}(\rho uv) + \frac{\partial}{\partial x} \tau_{xx} + \frac{\partial}{\partial y} \tau_{yx} = 0 \quad (2.2)$$

$$\frac{\partial}{\partial t}(\rho v) + \frac{\partial}{\partial x}(\rho uv) + \frac{\partial}{\partial y}(\rho + \rho vv) + \frac{\partial}{\partial x} \tau_{xy} + \frac{\partial}{\partial y} \tau_{yy} = 0 \quad (2.3)$$

The numerical solution of this system of equations present following problems:

- The convective terms of the momentum equations contain nonlinear quantities.
- All three equations are intricately coupled because every velocity component appears in each momentum equation and continuity equation.
- The most complex issue to resolve is the role played by the pressure. It appears in both momentum equations, but there is evidently no (transport or other) equation for pressure.

If the pressure gradient is known, the process of obtaining discretised equations for velocities from corresponding momentum equations is similar to that for any other scalar variable governed by convection-diffusion mechanism. But in general purpose flow computations, we wish to calculate the pressure field as part of the solution. So the pressure gradient is not known beforehand. If the flow is compressible the continuity equation can be used as a transport equation for density and, in addition to the Navier-Stokes equations, the energy equation is invoked as a transport equation for temperature. The pressure may then be obtained from the equation of state, $p = p(\rho, T)$. However, if the flow is incompressible the density is constant with respect to both time and space (i.e. $\frac{D\rho}{Dt} = 0$), and hence by definition not linked to the pressure.

Now, in the recent past compressible flow applications to aerodynamics have caused great deal of attention to be focused on development of methods for numerical solution of compressible flow equations. Therefore, it is of significant interest to be able to use some of these compressible flow algorithms for solving incompressible flow equations. The major difference between the equations of compressible and incompressible flows is their mathematical character. Hence if the methods for compressible flow are to be used to compute incompressible flow, the character of the equation will need to be modified. The difference in character between compressible and incompressible flows can be traced to the

lack of time derivative term in the incompressible continuity equation. The compressible version of the continuity equation contains the time derivative of density. The most straightforward means of giving the incompressible equations compressible character is to insert the time derivative of density into the continuity equations. Since density is constant for incompressible flows adding $\frac{\partial \rho}{\partial t}$ i.e. using compressible equation, is not possible. Also time derivative of the velocity component exist in momentum equations, so they are not suitable choice to fulfill the purpose. That leaves the time derivative of pressure as the clear choice. In the artificial compressibility method originally introduced by Chorin (1968) pressure p is related with artificial density ρ by the artificial equation of state

$$p = \delta \rho \quad (2.4)$$

with the objective of solving the steady state incompressible Navier-Stokes equations

$$\frac{\partial u}{\partial x} + \frac{\partial v}{\partial y} = 0 \quad (2.5)$$

$$\frac{\partial}{\partial x}(p' + uu) + \frac{\partial}{\partial y}(uv) + \frac{\partial}{\partial x}\tau_{xx} + \frac{\partial}{\partial y}\tau_{yx} = 0 \quad (2.6)$$

$$\frac{\partial}{\partial x}(uv) + \frac{\partial}{\partial y}(p' + vv) + \frac{\partial}{\partial x}\tau_{xy} + \frac{\partial}{\partial y}\tau_{yy} = 0 \quad (2.7)$$

where p' is the pressure normalized with density, shear-stress

$\tau_{xx} = -2\nu \frac{\partial u}{\partial x}$, $\tau_{yy} = -2\nu \frac{\partial v}{\partial y}$, $\tau_{xy} = -\nu \left(\frac{\partial u}{\partial y} + \frac{\partial v}{\partial x} \right)$ and ν is kinematic viscosity. Here

τ is an auxiliary variable whose role is analogous to that of time in a compressible flow problem. The basic idea was to replace equations (2.5), (2.6) and (2.7) by

$$\frac{1}{\delta} \frac{\partial p}{\partial \tau} + \left(\frac{\partial u}{\partial x} + \frac{\partial v}{\partial y} \right) = 0 \quad (2.8)$$

$$\frac{\partial u}{\partial \tau} + \frac{\partial}{\partial x}(p' + uu) + \frac{\partial}{\partial y}(uv) + \frac{\partial}{\partial x}\tau_{xx} + \frac{\partial}{\partial y}\tau_{yx} = 0 \quad (2.9)$$

$$\frac{\partial v}{\partial \tau} + \frac{\partial}{\partial x}(uv) + \frac{\partial}{\partial y}(p' + vv) + \frac{\partial}{\partial x}\tau_{xy} + \frac{\partial}{\partial y}\tau_{yy} = 0 \quad (2.10)$$

where, δ is an arbitrary real positive parameter called artificial compressibility or pseudo-compressibility parameter whose value is key to the performance of the method. These two terms, artificial compressibility and pseudo-compressibility, are used interchangeably in the literature. As time t in equations (2.8) to (2.10) no longer represent a true physical time in this formulation, now onwards it is replaced with τ . With the above modification Chorin (1967) transformed the elliptic incompressible equations to a hyperbolic compressible system, which can be solved by standard, implicit time-marching methods (Madsen et. al., (2006)) usually applied for solving the compressible flow algorithm.

In the steady state formulation the above equations (2.8) to (2.10) are advanced in the artificial time dimension (pseudo time, τ) until the artificial time derivative goes to zero and the divergence of velocity in equation (2.8) converges to a specified tolerance. When this happens the solution of the original continuity (2.5) and momentum equation (2.6) and (2.7) for incompressible flow is recovered. For an unsteady problem this must be done in every time step. The modified continuity equation does not exhibit any physical meaning until steady state is reached. Addition of a time derivative of the pressure to continuity equation means that we are no longer solving the true incompressible equations. As a result the time history generated cannot be accurate, but on convergence this time derivative becomes zero and the solution satisfies incompressible continuity condition. Chorin first proposed this approach and various versions have been adopted since then.

2.1 Literature survey on artificial compressibility method

A large volume of literature is available on the subject of Artificial Compressibility Method (ACM). However in this review the main aim is to restrict the discussion to relevant utility applications.

Rizzi and Erikson (1985) have applied Chorin's artificial compressibility method to strictly inviscid incompressible flow. The modified system of equations was solved by a time marching finite volume method using an explicit three-stage Runge-Kutta time stepping scheme. They also investigated the transient calculation as the artificial compressibility method approaches steady flow asymptotically in time. Their computed results include both irrotational and rotational solutions. The two dimensional examples include inviscid incompressible flow past a circular cylinder and NACA-0012 airfoil at 5° angle of attack. Incompressible flow around a 70° -swept wing of zero thickness and unit length at 20° angle of attack was presented as a three-dimensional solution test case.

Chang et. al. (1988) have supported artificial compressibility method over other solution methods because of its efficiency in solving three-dimensional real world problems.

Gorski (1988 a, b, c) developed a third-order accurate upwind differential TVD (Total Variation Diminishing) scheme to discretize the convective terms coupled with standard central differences for the viscous diffusion terms of the two-dimensional Navier-Stokes equations using pseudo-compressibility. The equations were solved implicitly using approximate factorization with an implicit multi-grid technique for convergence acceleration. The value of artificial compressibility parameter was taken as unity. Results and convergence histories were presented for an idealized inviscid cascade, a turbulent flat plate cascade and the turbulent flow over a double circular cascade.

Hirsch and Hakimi (1995) in their paper have shown how the general form of preconditioning equations can be reduced to the Chorin's approach to artificial compressibility. Three example problems were demonstrated i.e. inviscid flow over a cylinder, a three-dimensional viscous flow in a 90 degree curved bend for low Mach number flows, lid-driven and buoyancy driven viscous flow in a square

cavity. The authors have used explicit Runge–Kutta time stepping and a central space discretization for computing both inviscid as well as viscous flows.

Rogers and Kwak (1987, 1990, 1991a, 1991b) have solved two-dimensional incompressible Navier-Stokes equation using artificial compressibility method. They have performed sub-iterations in each pseudo time step to confirm continuity. An upwind differencing scheme based on flux-difference splitting was used to compute the convective terms. Based on the sign of the local Eigen values of the relaxation scheme, the upwind differencing was used to solve the equations. A number of numerical tests were done to determine the suitable value of the artificial compressibility parameter. Good agreement between the computed solutions and the analytical test case results were observed. They have extended the methodology to three-dimensional problems also. The benchmark test problems that were successfully computed include steady state solution of flow through a square duct with a 90° bend, unsteady flow over a circular cylinder and unsteady flow through an artificial heart configuration with moving boundary.

Dick (1988) applied the flux vector splitting method to the convective part of the steady Navier Stokes equations. He has introduced partial up-wind differences in the first order part and central differences in the second order part of the equations. Thus a set of discrete equations were obtained and solved by the relaxation method. The flux vector splitting technique was used for the first-order equations. An up-wind discretization of the split form was obtained when the positive terms were discretized by backward differences and the negative terms by forward differences. The value of artificial compressibility was chosen based on numerical test. A test problem for backward facing step has been solved and validated.

Kwak (1986) have developed an implicit finite difference code to solve the incompressible Navier-Stokes equation in a three-dimensional curvilinear coordinate system. The pressure field solution was based on the artificial

compressibility approach of Chorin. The solution procedure employed was an implicit approximate factorization scheme. A fourth order explicit and a second order implicit smoothing term was required to make algorithm stable. Example problems demonstrated were flow past a circular cylinder, channel flow in two-dimensional rectangular duct with 45° bend and flow in a three-dimensional annular duct with a 180° bend.

Several variations of the artificial compressibility method (ACM) have been reported in the literature. Steger and Kutler (1977), Kwak *et al.* (1986,2005), and Rogers *et al.* (1990) used an implicit approximate factorization scheme by Beam and Warming (1976). Rogers *et al.* (1991) used higher-order flux splitting techniques. Ramshaw and Mousseau (1990) accelerated convergence of the ACM method by introducing an artificial bulk viscosity to dissipate the artificial sound waves more rapidly. Further, Turkel (1987) introduced artificial time derivatives in the momentum equations to allow for faster convergence. Fast implicit schemes developed for compressible flows, such as the approximate-factorization scheme by Beam and Warming (1976) and the implicit lower upper symmetric Gauss-Seidel (LU-SGS or Lower Upper Symmetric Gauss Seidel) scheme was implemented to solve the hyperbolic-parabolic system of equations in ACM methods. Various applications that evolved from this concept have been reported for obtaining steady state solutions i.e. Steger and Kutler (1977), Kwak *et al.* (1986), Chang *et al.* (1988), Choi and Merkel (1985,1993). Rosenfield and Kwak (1991) extended the ACM to solve unsteady problems. Merkle and Athavale (1987), Soh and Goodrich (1988) were some of the first to extend the ACM to the solution of the unsteady incompressible Navier-Stokes equations. Nithiarasu (2003) has presented an efficient artificial compressibility scheme based on the characteristics based split (CBS) method for incompressible flows using finite element method (FEM) framework. To obtain time dependent solutions using this method an iterative procedure can be applied in each physical time step such that the continuity equation is satisfied. Merkle and Athavale (1987) and Rogers and Kwak (1991) reported successful computations using this approach. Kwak *et. al.* (1986) has been instrumental in developing the

INS2D and INS3D family of codes, which were based on the artificial compressibility method.

2.2 Significance of artificial compressibility parameter δ

Physically, equation (2.8) signifies that waves of finite speed are introduced into the incompressible flow field as a medium to distribute the pressure. For a truly incompressible flow, the wave speed is infinite, whereas the speed of propagation of these pseudo-waves depends on the magnitude of artificial compressibility. Additionally, in a true incompressible flow, the pressure field is affected instantaneously by any disturbances in the flow field, but with artificial compressibility, there is a time lag between the flow disturbance and its effect on the pressure field, Kwak (2005). Ideally, the value of the artificial compressibility is chosen to be as high as the particular choice of algorithm allows, so that the incompressibility is recovered quickly. This must be done without decreasing the accuracy and stability property of the numerical method implemented. On the other hand if, the artificial compressibility is chosen such that these waves travel too slowly, then the variation of the pressure field accompanying these waves will be very slow. Another way of looking at this is that as the Mach number goes to zero, the governing equations become the incompressible Navier-Stokes equations, which contain no time derivative of pressure. The method of artificial compressibility introduces a finite speed of sound into the incompressible Navier-Stokes equation, which has an infinite speed of sound. The artificial compressibility algorithm requires the selection of a parameter, which defines the artificially introduced speed of sound. The value of this parameter can vary by four orders of magnitude (Ramshaw (1990)) depending on the flow and the physical time step. Thus, the optimal value of this parameter has to be chosen by trial and error, and, given the large range of values that this parameter can take; several trial solutions must be attempted. This will interfere with the timely development of the viscous boundary layer. In viscous flow the behavior of the boundary layer is very sensitive to the streamwise pressure gradient, especially when the boundary layer is separated.

If separation is present, a pressure wave traveling with finite speed will cause a change in the local pressure gradient, which will affect the location of the flow separation. This change in separated flow will cause a feed back to the pressure field, possibly preventing convergence to a steady state. The test case of viscous flow on a backward step to understand the effect of δ on the flow separation zone has been planned. Especially for internal flow, the viscous effect is important for the entire flow field, and the interaction between the pseudo-pressure waves and the viscous flow field becomes very important.

Some literatures suggest a mathematical way to select δ (without doing trial and error), the only adjustable parameter required by the pseudo-compressibility method. Since the convergence of the method is very sensitive to this parameter, selection of this parameter is quite critical. Dimensional analysis shows that δ is a function of square of speed. One of the early attempts to select δ was made by Turkel (1987). Turkel has suggested the value of the parameter δ to be

$$\delta = k_1 \max[u^2, v^2, \varepsilon_s] \quad (2.11)$$

where k_1 is an arbitrary real positive constant and ε_s is introduced to avoid ill-conditioning near stagnation points. The value of k_1 for optimum convergence and for inviscid flow was suggested of the order of unity, Rogers (1991). The value of δ for viscous flow has been suggested by Hirsch and Hakimi (1995, 1997) as

$$\delta = k_2 u_{\text{ref}}^2 \quad (2.12)$$

where k_2 is a real positive constant which depends on the Reynolds number. U_{ref} can be taken as the free stream velocity for external flows whereas for internal flows it can be taken as the maximum inlet velocity. The value of k_2 can be taken as order of unity for Reynolds number >1000 . For lower value of Reynolds number k_2 should increase as the Reynolds number decreases and this value of k_2 can vary over several orders of magnitude as the Reynolds number decreases from thousand to one. Later Turkel (1987,1999) has modified his earlier definition of δ and suggested the value of ε of the order of unity. This value almost falls in

line with Hirsch and Hakimi (1995,1997) for external flows. Agarwal and Mandal (2001) has used the Turkel's expression for inviscid computation and for viscous computation, the expression given by Hirsch and Hakimi (1995) to compute the value of artificial compressibility parameter δ .

2.3 Values of artificial compressibility parameter δ

The artificial compressibility method has a significant drawback lying in the difficulty of choosing the value of artificial compressibility parameter δ , improper choice of which leads to slow convergence or even divergence. For acceptable performance, the artificial compressibility method requires trial and error adjustment procedure to determine the value of the artificial compressibility parameter, which is a time consuming process. In this section the different method to determine the value of this parameter available in the literature has been discussed.

The incompressible modified continuity equation (2.8) due to artificial compressibility method and momentum equations (2.9) and (2.10) respectively can be written in primitive variable form extended to three-dimension as

$$\frac{\partial p}{\partial \tau} + \frac{\partial u}{\partial x} + \frac{\partial v}{\partial y} + \frac{\partial w}{\partial z} = 0 \quad (2.13)$$

$$\frac{\partial u}{\partial \tau} + u \frac{\partial u}{\partial x} + v \frac{\partial u}{\partial y} + w \frac{\partial u}{\partial z} = -\frac{\partial p}{\partial x} + \frac{1}{\text{Re}_L} \left(\frac{\partial^2 u}{\partial x^2} + \frac{\partial^2 u}{\partial y^2} + \frac{\partial^2 u}{\partial z^2} \right) \quad (2.14)$$

$$\frac{\partial v}{\partial \tau} + u \frac{\partial v}{\partial x} + v \frac{\partial v}{\partial y} + w \frac{\partial v}{\partial z} = -\frac{\partial p}{\partial y} + \frac{1}{\text{Re}_L} \left(\frac{\partial^2 v}{\partial x^2} + \frac{\partial^2 v}{\partial y^2} + \frac{\partial^2 v}{\partial z^2} \right) \quad (2.15)$$

$$\frac{\partial w}{\partial \tau} + u \frac{\partial w}{\partial x} + v \frac{\partial w}{\partial y} + w \frac{\partial w}{\partial z} = -\frac{\partial p}{\partial z} + \frac{1}{\text{Re}_L} \left(\frac{\partial^2 w}{\partial x^2} + \frac{\partial^2 w}{\partial y^2} + \frac{\partial^2 w}{\partial z^2} \right) \quad (2.16)$$

where $\text{Re}_L = \frac{v_\infty L}{\nu}$ being the Reynolds number and L =Characteristics length. In

artificial compressibility method, the continuity equation is modified to include an artificial compressibility term, which vanishes when the steady state is reached.

Here ρ is an artificial density, equated to the product of inverse of artificial compressibility factor δ and pressure by the artificial equation of state (reference equation 2.4),

$$\rho = \delta^{-1}p \quad (2.17)$$

where, $\frac{\partial \rho}{\partial \tau} \rightarrow 0$ at the steady state and τ is a fictitious time. Since this is an artificial equation of state, then $\delta^{1/2}$ plays the role of an artificial sound speed. Here it is important to note that at steady state the solution is independent of ρ and τ . Now substituting equation (2.17) into equation (2.13), we can apply a suitable numerical technique to the resulting equations and march the solution in τ to obtain a final steady-state incompressible solution. Obviously, this technique is applicable only to steady-flow problems, since it is not time accurate.

Now we can write the incompressible Navier Stokes system of equations (2.13-2.16) along with the artificial equation of state (2.17) in the generalized form

$$\frac{\partial \bar{\mathbf{u}}}{\partial \tau} + \frac{\partial \bar{\mathbf{e}}}{\partial x} + \frac{\partial \bar{\mathbf{f}}}{\partial y} + \frac{\partial \bar{\mathbf{g}}}{\partial z} = \frac{1}{\text{Re}_L} \left(\frac{\partial^2}{\partial x^2} + \frac{\partial^2}{\partial y^2} + \frac{\partial^2}{\partial z^2} \right) [\mathbf{D}] \bar{\mathbf{u}} \quad (2.18)$$

where,

$$\bar{\mathbf{u}} = \begin{bmatrix} p \\ u \\ v \\ w \end{bmatrix} \quad \bar{\mathbf{e}} = \begin{bmatrix} \delta u \\ p + (u)^2 \\ uv \\ uw \end{bmatrix}$$

$$\bar{\mathbf{f}} = \begin{bmatrix} \delta v \\ uv \\ p + (v)^2 \\ vw \end{bmatrix} \quad \bar{\mathbf{g}} = \begin{bmatrix} \delta w \\ uw \\ vw \\ p + (w)^2 \end{bmatrix} \quad (2.19)$$

$$\text{and, } [\mathbf{D}] = \begin{bmatrix} 0 & 0 & 0 & 0 \\ 0 & 1 & 0 & 0 \\ 0 & 0 & 1 & 0 \\ 0 & 0 & 0 & 1 \end{bmatrix} \quad (2.20)$$

Now defining Jacobians,

$$\begin{aligned}
[A_1] = \frac{\partial \mathbf{e}}{\partial \mathbf{u}} &= \begin{bmatrix} 0 & \delta & 0 & 0 \\ 1 & 2u & 0 & 0 \\ 0 & v & u & 0 \\ 0 & w & 0 & u \end{bmatrix} & [A_2] = \frac{\partial \mathbf{f}}{\partial \mathbf{u}} &= \begin{bmatrix} 0 & 0 & \delta & 0 \\ 0 & v & u & 0 \\ 1 & 0 & 2v & 0 \\ 0 & 0 & w & v \end{bmatrix} \\
[A_3] = \frac{\partial \mathbf{g}}{\partial \mathbf{u}} &= \begin{bmatrix} 0 & 0 & 0 & \delta \\ 0 & w & 0 & u \\ 0 & 0 & w & v \\ 1 & 0 & 0 & 2w \end{bmatrix} & & (2.21)
\end{aligned}$$

Hence the equation (2.18) can be rewritten as

$$\frac{\partial \bar{\mathbf{u}}}{\partial \tau} + [A_1] \frac{\partial \bar{\mathbf{u}}}{\partial x} + [A_2] \frac{\partial \bar{\mathbf{u}}}{\partial y} + [A_3] \frac{\partial \bar{\mathbf{u}}}{\partial z} = \frac{1}{\text{Re}_L} \left(\frac{\partial^2}{\partial x^2} + \frac{\partial^2}{\partial y^2} + \frac{\partial^2}{\partial z^2} \right) [\mathbf{D}] \bar{\mathbf{u}} \quad (2.22)$$

Now in order to evaluate the eigenvalues of A_i we put

$$\det |A_i - \lambda_i I| = 0 \quad (2.23)$$

where the eigenvalues of $[A_i]$ ($i=1,2,3$) are

$$\left(u, u, u \pm \sqrt{u^2 + \delta} \right), \left(v, v, v \pm \sqrt{v^2 + \delta} \right), \left(w, w, w \pm \sqrt{w^2 + \delta} \right) \quad (2.24)$$

respectively. The idea is to maintain low enough δ (close to the convective velocity) to overcome stiffness associated with a disparity in the magnitudes of the eigenvalues, but high enough such that pressure waves (moving with infinite speed at incompressible limit) be allowed to travel far enough to balance viscous effects. As a result, the conservation of mass or incompressibility condition is assured by means of an artificial compressibility. In this process it is possible to obtain the correct pressure distributions. Although the artificial equation of state suggests that $\delta^{1/2}$ is an artificial speed of sound, the eigenvalues above indicate that the effective acoustic wave speeds are really the quantities under the radicals in the eigenvalues above ($\sqrt{u^2 + \delta}$, for example), which are functions of the velocity components as well as δ . From the point of view of linear algebra, the finite difference algebraic equations resulting from equation (2.18) are well conditioned (Chung (2002)) with a proper choice of δ . This is due to the well-conditioned eigenvalues given by equation (2.24).

Artificial compressibility relaxes the strict requirement to satisfy mass conservation in each time step. Chang and Kwak (1988) reported details of artificial compressibility, and suggested some useful guidelines for choosing the artificial compressibility parameter. At first sight, it might appear that δ is relatively easy to choose. For instance, $\sqrt{\delta}$ could be chosen to be equal to some representative convective velocity as in Marx (1994). It is also possible for $\sqrt{\delta}$ not to be a constant over the entire flow field but instead chosen to be equal to a local velocity (Stegar (1977)). Computational experience has shown (McHugh (1995)) that this is not the case, and that δ can vary from 1 to 10000 depending on the flow and the pseudo and physical time step. If all else is kept constant, as δ is increased a smaller pseudo time step must be taken and the ratio of the momentum residuals to the residual of the continuity equation increases. Since time accuracy in pseudo time is of no concern, the time derivatives in equation (2.8-2.10) should be discretized using methods chosen to maximize efficiency and robustness. Local time stepping, in which the equation is advanced at different rates in pseudo time depending on spatial position, can be used. This improves the convergence rate by not restricting the global pseudo time step to the minimum required locally.

From the eigenvalues obtained in equation (2.24) the transient solution of Navier-Stokes equations through ACM can be thought of as being decomposed into different modes of the form $e^{-\lambda_i t}$, etc. Thus for large values of δ , different modes will decay at significantly different rates and the system of equation (2.18) is said to be stiff. If an explicit algorithm were used to march equation (2.18) in time the stiffness associated with large values of δ would show up as a severe stability restriction on Δt . This is avoided by using an implicit algorithm. However, Stegar and Kutler (1977) recommended that

$$\delta < \frac{1}{\Delta t} \quad (2.25)$$

to maintain first order time accuracy in the implicit algorithm. If δ is made too small the continuity equation (2.13) will not be satisfied sufficiently accurately

with a destabilizing effect on the transient solution. Kwak et al. (1986) provide the following lower bounds for δ . For a simple channel flow the requirements of pressure waves to propagate much faster than the vorticity spreads, δ is given by

$$\delta \geq \left[1 + \left(\frac{4}{\text{Re}} \right) \left(\frac{x_{\text{ref}}}{x_{\delta}} \right)^2 \left(\frac{x_L}{x_{\text{ref}}} \right) \right]^2 - 1, \quad (2.26)$$

and for turbulent flow,

$$\delta \geq \left[1 + \left(\frac{1}{\text{Re}_t} \right) \left(\frac{x_{\text{ref}}}{x_{\delta}} \right) \left(\frac{x_L}{x_{\text{ref}}} \right) \right]^2 - 1 \quad (2.27)$$

where, x_L is the distance between inlet and outlet, x_{δ} is half distance between two walls and x_{ref} is the reference length. Re_t is the Reynolds number based on the turbulent eddy viscosity. Kwak et al. recommended $0.1 \leq \delta \leq 10$, for the example problem of flow past a circular cylinder at $\text{Re}=40$.

The formulation of artificial compressibility method revives a structure resembling the compressible equations by inserting artificial compressibility in the derivative of density with respect to the pressure. Within the framework of a two-dimensional analysis, the non-conservative form of the mass continuity equation (2.1) can be written as

$$\frac{\partial \rho}{\partial \tau} + u \frac{\partial \rho}{\partial x} + v \frac{\partial \rho}{\partial y} + \rho \left(\frac{\partial u}{\partial x} + \frac{\partial v}{\partial y} \right) = 0 \quad (2.28)$$

Having relaxed the incompressibility constraint, the continuity equation is perturbed as

$$\frac{\partial \rho}{\partial p} \left(\frac{\partial p}{\partial \tau} + u \frac{\partial p}{\partial x} + v \frac{\partial p}{\partial y} \right) + \rho \left(\frac{\partial u}{\partial x} + \frac{\partial v}{\partial y} \right) = 0 \quad (2.29)$$

where $\rho = \rho(p)$. Upon rearranging, equation (2.29) yields

$$\frac{\partial p}{\partial \tau} + u \frac{\partial p}{\partial x} + v \frac{\partial p}{\partial y} + \rho c^2 \left(\frac{\partial u}{\partial x} + \frac{\partial v}{\partial y} \right) = 0 \quad (2.30)$$

where c is denominated herein as the artificial sound speed or perturbation parameter recognized by

$$\frac{1}{c^2} = \frac{\partial \rho}{\partial p} \quad (2.31)$$

Reverting to the justification of continuity modification, it can be immediately seen that the artificial sound speed must be sufficiently large to have a significant regularizing effect, and must be as small as possible to minimize perturbations on the incompressibility equation. To reconcile this criterion, c is estimated by Rahman and Sikoken (2007)

$$c = \delta \sqrt{\max \left[(u^2 + v^2), \frac{1}{2} U_{\text{ref}}^2 \right]} \quad (2.32)$$

where U_{ref} represents a reference velocity and δ is the compressibility parameter. Evidently, c depends on δ , influencing the convergence rate and stability of the solution method. Rahman and Sikoken (2007) have recommended values of δ in the range of 1-10, for better convergence to the steady state at which the mass conservation is enforced.

2.4 Governing equations of ACM in flux form

Combining equation (2.8) with the momentum equation (2.9-2.10) for the incompressible Navier-Stokes equations results in the following system in Cartesian coordinates and replacing p' with p for clarity

$$\frac{\partial}{\partial \tau}(\mathbf{U}) + \frac{\partial}{\partial x}(\mathbf{GX}_I + \mathbf{GX}_V) + \frac{\partial}{\partial y}(\mathbf{GY}_I + \mathbf{GY}_V) = 0 \quad (2.33)$$

where

$$\mathbf{U} = \begin{bmatrix} p \\ u \\ v \end{bmatrix}, \quad \mathbf{GX}_I = \begin{bmatrix} \delta u \\ u^2 \\ uv \end{bmatrix}, \quad \mathbf{GY}_I = \begin{bmatrix} \delta v \\ uv \\ v^2 \end{bmatrix},$$

$$\mathbf{GX}_V = \begin{bmatrix} 0 \\ \tau_{xx} + p \\ \tau_{xy} \end{bmatrix}, \quad \mathbf{GY}_V = \begin{bmatrix} 0 \\ \tau_{yx} \\ \tau_{yy} + p \end{bmatrix},$$

$$\tau_{xx} = -2\nu \frac{\partial u}{\partial x}, \quad \tau_{yy} = -2\nu \frac{\partial v}{\partial y}, \quad \tau_{xy} = \tau_{yx} = -\nu \left(\frac{\partial u}{\partial y} + \frac{\partial v}{\partial x} \right) \quad (2.34)$$

where p is the pressure. G_{X_I} and G_{Y_I} are the x and y component of inviscid flux while G_{X_V} and G_{Y_V} are the x and y components of viscous flux respectively.

2.5 Summary

In this chapter incompressible flow simulation using artificial compressibility method has been discussed, and a literature survey on the artificial compressibility method has been presented. Then the significance and value of the artificial compressibility parameter δ has been discussed. Finally the governing equation of artificial compressibility method in flux form has been presented. In the next chapter mesh less method have been discussed in details.

CHAPTER 3

Meshless Code Development

3.0 Literature survey on meshless methods

In the past two decades considerable amount of research has been carried out in the field of meshless CFD, popularly referred to as “Gridless CFD” (MacCormack (1993)). One of the earliest works pertains to the paper on “Generalized finite difference method” by Chung (1981). The fundamental idea explored in this work, related to the use of Taylor series expansion, for obtaining the discrete approximation of the derivatives at any given point, has not undergone any change. On the other hand, at the implementation level significant modifications have been experimented with, leading to the success/failure of the aforesaid procedure. As example we can cite the work of Deshpande et al. (1998) and Batina (1993). Both employ a least-squares procedure for solving the resulting over specified system of equations in contrast to the work of Chung (1981), where a stencil of grid points just adequate to solve for the derivatives appearing in the truncated Taylor series is employed. While the work of Deshpande et al. (1989) deals with an upwind implementation based on kinetic theory of gases, resulting in least-squares kinetic upwind method (LSKUM) (Deshpande et al. (1998)), that of Batina (1993) is based on a centered scheme using artificial dissipation. Particularly LSKUM has been applied for many two-dimensional inviscid flows (Ramesh (2001)) and was shown to yield notable solutions even for discontinuous flows. The LSKUM has also been extended to viscous flows. Mahendra (2003) have used the Chapman-Enskog distribution function in LSKUM to simulate viscous rotating flow. Sridar (2003) presented a new Least-Squares-based Upwind Finite Difference method (Balakrishnan (1999a, 1999b, 2000)) referred to as LSFU. The new method uses a global stencil of grid points. The method due to Sridar (2003) has the flexibility to choose between different flux formulas like Roe (1981), van Leer

(1982, 1991), KFVS (1994), AUSM (1993), etc. The other interesting development in this area is due to Morinishi (2000a, 2000b) and Lohner et. al (2002). They have used "weighted least-squares" approach to find the derivatives at a node. Other grid free methods outside the realm of finite difference method, for fluid flow computations, are Reproducing Kernel Particle Method (RKPM) due to Liu et al. (1995) and Meshless Local Petrov–Galerkin (MLPG) due to Atluri (2001). The RKPM is also a meshless particle (Lagrangian) method like Cubic Interpolation with Volume/Area co-ordinates (CIVA) due to Tanaka (1999). The CIVA uses cubic interpolation pseudo-particle (CIP) algorithm to obtain high accuracy.

The following numerical methods are generally considered to fall within the general class of "meshless" methods. Acronyms are provided in parentheses.

Smoothed-Particle Hydrodynamics (SPH) (Monaghan (1988)) is a computational method used for simulating fluid flows. It has been used in many fields of research, including astrophysics and oceanography. It is a mesh-free Lagrangian method (where the co-ordinates move with the fluid), and the resolution of the method can easily be adjusted with respect to variables such as the density. The SPH method works by dividing the fluid into a set of discrete elements, referred to as particles. These particles have a spatial distance (known as the "smoothing length", typically represented in equations by h), over which their properties are "smoothed" by a kernel function. This means that any physical quantity of any particle can be obtained by summing the relevant properties of all the particles which lie within the range of the kernel.

The Diffuse Element Method (DEM) (Nayroles (1992)), is a meshless method. It was developed by Nayroles, Touzot and Villon in 1992. It is in concept rather similar to the much older SPH. In the paper they describe a "diffuse approximation method", a method for function approximation from a given set of points. Using this function approximation method, PDEs and thus fluid dynamics problems can be solved. For this, they coined the term Diffuse Element Method

(DEM). Advantages over FEM are that DEM doesn't rely on a grid, and is more precise in the evaluation of the derivations of the reconstructed functions.

The Particle-In-Cell (PIC) method by Harlow (1964) refers to a technique used to solve a certain class of PDEs. In this method, individual particles (or fluid elements) in a Lagrangian frame are tracked in continuous phase space, whereas moments of the distribution such as densities and currents are computed simultaneously on Eulerian (stationary) mesh points. PIC methods were already in use as early as 1955.

The Material Point Method (MPM) (Sulsky (1994)) is an extension from the Particle-In-Cell (PIC) method in computational fluid dynamics to computational solid dynamics, and is FEM based particle method. It is primarily used for multiphase simulations, because of the ease of detecting contact without interpenetration. It can also be used as an alternative to dynamic FEM methods to simulate large material deformations, because there is no re-meshing required by the MPM. In the MPM, Lagrangian point masses, or material points, are moved through a Eulerian background mesh. At the end of each calculation cycle, a 'convective' step occurs, in which the mesh is reset to its original position, while material points remain in their current positions. There are two key differences between the PIC and MPM. The first one is that the MPM is formulated in the weak form similar to that for the FEM so that the FEM and MPM could be combined together for large-scale simulations. The second one is that history-dependent constitutive models could be formulated on the material points, which results in a robust spatial discretization method for multiphase and multi-physics problems.

The Moving Particle Semi-Implicit (MPS) (Koshizuka (1996,2001)) method is a computational method for the simulation of incompressible free surface flow. It is a macroscopic, deterministic particle method (Lagrangian meshless method) developed by Koshizuka and Oka (1996). The MPS method applies simplified differential models solely based on a local weighted averaging process without taking the gradient of a kernel function. In addition, the solution process of MPS

method differs to that of the original SPH method as the solutions to the PDEs are obtained through a semi-implicit prediction-correction process rather than the fully explicit one in original SPH method.

3.1 Least square based discretisation

The present work uses Least squares based discretisation, which is a meshless or grid free method. In case of finite difference methods the above equation is solved by discretising the various derivatives along the co-ordinate directions. Finite volume method is based on integral form of governing equations. However if we are given an arbitrary distribution of points without any grid structure associated with these points, it will be difficult to discretise the

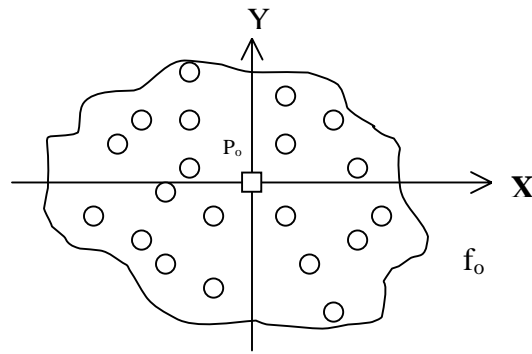


Figure 3.1: Typical connectivity around point P_o

derivatives. With the least square approach spatial derivatives f_x, f_y of f can be discretised in terms of the data at the neighbouring points or nodes. If we consider arbitrary n points (in general it has been observed, for a 2D or 3D calculation a minimum of two neighbouring nodes per quadrant are required for the least square based discretization) surrounding a point P_o as shown in figure 3.1 the analysis due to Ghosh (1996) shows that the Taylor series expansion around “ P_o ” for any quantity f gives $\Delta f_i = \Delta x_i f_{x_0} + \Delta y_i f_{y_0} + h.o.t.$ $i=1, \dots, n$, h.o.t.= higher order terms where $\Delta x_i = x_i - x_0$, $\Delta y_i = y_i - y_0$ and $\Delta f_i = f_i - f_0$. Here we can introduce weights based on the distance of a point from its neighbour. Hence square of error is given by

$$E = \sum_{i=1}^n w_i (\Delta f_i - f_{x_0} \Delta x_i - f_{y_0} \Delta y_i)^2 \quad (3.1)$$

where, w_i are positive weights. Now minimizing E w.r.t. f_{x_0} and f_{y_0} i.e. putting

$$\frac{\partial E}{\partial f_{x_0}} = \frac{\partial E}{\partial f_{y_0}} = 0$$

gives the following first order accurate least square formulae for

the gradients

$$\begin{aligned} f_{x_0}^{(1)} &= \frac{\sum w_i \Delta y_i^2 \sum w_i \Delta x_i \Delta f_i - \sum w_i \Delta x_i \Delta y_i \sum w_i \Delta y_i \Delta f_i}{\sum w_i \Delta x_i^2 \sum w_i \Delta y_i^2 - (\sum w_i \Delta x_i \Delta y_i)^2} \\ f_{y_0}^{(1)} &= \frac{\sum w_i \Delta x_i^2 \sum w_i \Delta y_i \Delta f_i - \sum w_i \Delta x_i \Delta y_i \sum w_i \Delta x_i \Delta f_i}{\sum w_i \Delta x_i^2 \sum w_i \Delta y_i^2 - (\sum w_i \Delta x_i \Delta y_i)^2} \end{aligned} \quad (3.2)$$

where, Σ represents the summation over all points in the neighbourhood $N(P_0)$ of P_0 . The formulae given in equation (3.2) can now be used to obtain the point values of f_{x_0} and f_{y_0} throughout the field. The formula to calculate second order accurate f_{x_0} and f_{y_0} is given in appendix A.

3.2 Incorporation of upwind scheme

In this section, how upwinding is enforced in least square based discretization method by stencil subdivision has been described. Consider a 2-D linear hyperbolic partial differential equation for scalar f .

$$\frac{\partial f}{\partial t} + u \frac{\partial f}{\partial x} + v \frac{\partial f}{\partial y} = 0 \quad (3.3)$$

The exact solution to this equation is given by

$$f(t + \Delta t, x, y, u, v) = f(t, x - u\Delta t, y - v\Delta t, u, v) \quad (3.4)$$

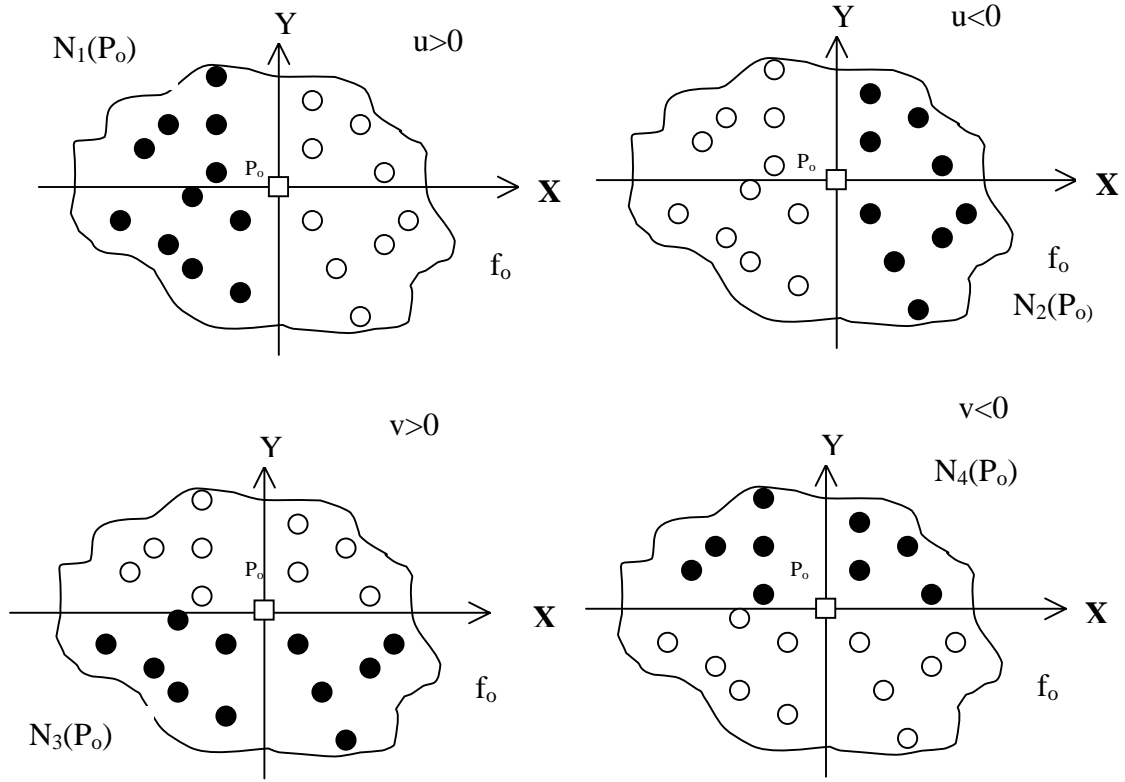


Figure 3.2: Stencil splitting for upwinding

The propagation of information to node P_0 depends upon location of node P_i relative to P_0 and the signs of u and v . If $u > 0$ then only the nodes to the left of P_0 will influence the solution at P_0 . Similarly If $u < 0$ then only the nodes to the right of P_0 will influence the solution at P_0 . Similar arguments show that for $v > 0$ the node below P_0 and for $v < 0$ the node above P_0 will influence the solution at P_0 . For developing any upwind scheme this signal propagation property should be taken into account. Hence the 2-D linear hyperbolic partial differential equation (3.3) for scalar f after enforcing upwinding becomes

$$\frac{\partial f}{\partial t} + \frac{u + |u|}{2} \left(\frac{\partial f}{\partial x} \right) + \frac{u - |u|}{2} \left(\frac{\partial f}{\partial x} \right) + \frac{v + |v|}{2} \left(\frac{\partial f}{\partial y} \right) + \frac{v - |v|}{2} \left(\frac{\partial f}{\partial y} \right) = 0 \quad (3.5)$$

Now replacing the spatial derivative in equation (3.5) by discrete least square approximation we get

$$\frac{\partial U}{\partial t} + \frac{u + |u|}{2} \{f_{x_0}^{(1)}\}_{N_1(P_0)} + \frac{u - |u|}{2} \{f_{x_0}^{(1)}\}_{N_2(P_0)} + \frac{v + |v|}{2} \{f_{y_0}^{(1)}\}_{N_3(P_0)} + \frac{v - |v|}{2} \{f_{y_0}^{(1)}\}_{N_4(P_0)} = 0 \quad (3.6)$$

This indicates that least square evaluation of derivative $\left\{f_{x_0}^{(1)}\right\}$ at node P_0 for $u>0$ should use data at nodes to the left of P_0 i.e. based on sub stencil $N_1(P_0)$ and is represented as $\left\{f_{x_0}^1\right\}_{N_1(P_0)}$ for $u>0$, $\left\{f_{x_0}^1\right\}_{N_2(P_0)}$ for $u <0$, $\left\{f_{y_0}^1\right\}_{N_3(P_0)}$ for $v >0$, $\left\{f_{y_0}^1\right\}_{N_4(P_0)}$ for $v <0$.

Therefore based on first order least square update formulation we get the final state update formula for ACM

$$\text{or, } \mathbf{U}^{n+1} = \mathbf{U}^n - \Delta\tau \left[\begin{array}{c} \left\{ \frac{\partial \mathbf{GX}^+}{\partial \mathbf{x}} \right\}_{N_1(P_0)} + \left\{ \frac{\partial \mathbf{GX}^-}{\partial \mathbf{x}} \right\}_{N_2(P_0)} \\ + \left\{ \frac{\partial \mathbf{GY}^+}{\partial \mathbf{y}} \right\}_{N_3(P_0)} + \left\{ \frac{\partial \mathbf{GY}^-}{\partial \mathbf{y}} \right\}_{N_4(P_0)} \end{array} \right] \quad (3.7)$$

where,

$$\begin{aligned} \left\{ \frac{\partial}{\partial \mathbf{x}} (\mathbf{GX}^+) \right\}_{N_1(P_0)}^n &= \left[\frac{\sum_i \Delta y_i^2 \sum_i \Delta x_i \Delta (\mathbf{GX}^+)_i^n - \sum_i \Delta x_i \Delta y_i \sum_i \Delta y_i \Delta (\mathbf{GX}^+)_i^n}{\sum_i \Delta x_i^2 \sum_i \Delta y_i^2 - (\sum_i \Delta x_i \Delta y_i)^2} \right]_{i \in N_1(P_0)} \\ \left\{ \frac{\partial}{\partial \mathbf{x}} (\mathbf{GX}^-) \right\}_{N_2(P_0)}^n &= \left[\frac{\sum_i \Delta y_i^2 \sum_i \Delta x_i \Delta (\mathbf{GX}^-)_i^n - \sum_i \Delta x_i \Delta y_i \sum_i \Delta y_i \Delta (\mathbf{GX}^-)_i^n}{\sum_i \Delta x_i^2 \sum_i \Delta y_i^2 - (\sum_i \Delta x_i \Delta y_i)^2} \right]_{i \in N_2(P_0)} \\ \left\{ \frac{\partial}{\partial \mathbf{x}} (\mathbf{GY}^+) \right\}_{N_3(P_0)}^n &= \left[\frac{\sum_i \Delta x_i^2 \sum_i \Delta y_i \Delta (\mathbf{GY}^+)_i^n - \sum_i \Delta x_i \Delta y_i \sum_i \Delta x_i \Delta (\mathbf{GY}^+)_i^n}{\sum_i \Delta x_i^2 \sum_i \Delta y_i^2 - (\sum_i \Delta x_i \Delta y_i)^2} \right]_{i \in N_3(P_0)} \\ \left\{ \frac{\partial}{\partial \mathbf{x}} (\mathbf{GY}^-) \right\}_{N_4(P_0)}^n &= \left[\frac{\sum_i \Delta x_i^2 \sum_i \Delta y_i \Delta (\mathbf{GY}^-)_i^n - \sum_i \Delta x_i \Delta y_i \sum_i \Delta x_i \Delta (\mathbf{GY}^-)_i^n}{\sum_i \Delta x_i^2 \sum_i \Delta y_i^2 - (\sum_i \Delta x_i \Delta y_i)^2} \right]_{i \in N_4(P_0)} \end{aligned} \quad (3.8)$$

where,

$$\Delta (\mathbf{GX}^\pm)_i^n = (\mathbf{GX}^\pm)_i^n - (\mathbf{GX}^\pm)_0^n \text{ and } \Delta (\mathbf{GY}^\pm)_i^n = (\mathbf{GY}^\pm)_i^n - (\mathbf{GY}^\pm)_0^n.$$

The $\left\{ \frac{\partial}{\partial \mathbf{x}} (\mathbf{GX}^+) \right\}_{N_1(P_0)}^n$ indicates that least square evaluation of 1st order accurate (i.e., $n = 1$) derivative $\left\{ \frac{\partial}{\partial \mathbf{x}} (\mathbf{GX}^+) \right\}^n$. At node P_0 for $u>0$ should use data at nodes

to the left of P_o i.e. based on sub stencil $N_1(P_o)$, where i varies from 1 to maximum number of nodes in the sub stencil $N_1(P_o)$. A two-step formula to calculate second order accurate space derivatives used in the code has been elaborated in Appendix A. The expressions for the split fluxes are given in Appendix B, which are based on an ongoing work of Mahendra to be published shortly and preceded by the earlier research work of Junk and Rao (1999). In this work they have explored the relation between the lattice Boltzmann method for solving incompressible flow equations and the kinetic schemes, which are routinely used in computational fluid dynamics. Consequently a new discrete velocity method for the numerical solution of Navier–Stokes equations for incompressible fluid flow is presented by combining both the approaches. Junk and Rao (1999) have interpreted this as a pseudo-compressibility method.

3.3 Detailed features of the code

The main features of the code developed during the current work can be listed as following

- The code solves modified incompressible continuity and momentum (Navier Stokes) equations in two-dimensions using Chorin's (1968) artificial compressibility method.
- The grid information used by the code is an arbitrary distribution of grid points around any geometric configuration (popularly known as cloud of points) and connectivity set of each node using any method of grid generation (structured, unstructured, prismatic, Cartesian, chimera, hybrid, etc.)
- The code employs meshless method of least square based discretization to determine approximations to first order accurate space derivatives of any function f (state variables in the present case), $f_x^{(1)}$ and $f_y^{(1)}$ at any node P_o using data at neighbouring points.
- A two-step formula to calculate second order accurate space derivatives of any function f at the point o , $f_{x_o}^{(2)}$ and $f_{y_o}^{(2)}$ has been used in the code. In

the first step first order accurate $f_{x_0}^{(1)}$ and the modified difference $\Delta \tilde{f}_i$ is determined. In the second step using this modified difference the second order accurate $f_{x_0}^{(2)}$ is calculated.

- In determining the first or second order accurate space derivatives weighted least square based technique has been used where the weights are positive and given by

$$w_i = \frac{1}{(\Delta d)^m}$$

where $\Delta d = \sqrt{(x_i - x_o)^2 + (y_i - y_o)^2}$ is the distance between a point o and it's neighbor i, and $m=2,4,6,\dots$

- The addition of the time derivative of pressure to the continuity equation in the code creates a hyperbolic system of equations complete with artificial pressure waves of finite speed. When the solution converges to a steady state, a divergence free flow field is obtained.
- The code employs flux form of the governing equations and separates the total flux into inviscid and viscous part in both x and y direction.
- Derivatives of the inviscid fluxes at any node are calculated based on upwind stencil of neighbouring points while the derivatives of the viscous fluxes at any node are calculated based on full stencil of neighbouring points.
- The time step (Δt) used by the code is a function of minimum distance between a node and its neighbor (Δd) and artificial compressibility parameter δ as given by Chorin (1968).

$$\Delta t = 0.6 * \Delta d * \delta^{1/2} \tag{3.9}$$

- The optimal value of artificial compressibility parameter δ has been determined from a preliminary test computation using different models found in the literature.
- The code has the capability to adapt a cloud of points inside a meshless grid by finding gradient of any variable in the computation domain and adding points to that part of the domain.

3.4 Code details

The main steps of the code developed has been described below:

Step 1: The code requires input parameter file, grid file, output data file, restart data file and residue file.

Step 2: The input parameter file is read. Here parameters like flow Reynolds number, initial density, temperature, value of artificial compressibility parameter, maximum number of iterations, weight factor, total number of iterations and relaxation parameter are read.

Step 3: Grid information is read. Here x and y co-ordinate of each node, their connectivity information and location flag information are gathered.

Step 4: The flow field is initialized with initial boundary conditions and initial values of pressure, density, temperature and velocities. Alternatively for restart case these data are read from the restart file and the flow field is initialized with these restart data.

Step 5: The distance between each node and all it's neighbors in x and y-directions are calculated and stored in an array for future references.

Step 6: Inviscid split fluxes are calculated for all the points inside the domain.

Step 7: Velocity derivatives are calculated at all the points inside the domain.

Step 8: Unsplit viscous fluxes are calculated for all the points inside the domain.

Step 9: First order accurate space derivatives of the inviscid split fluxes using upwind stencil and viscous fluxes using full stencil are calculated for all the points inside the domain.

Step 10: Field variables are updated at all the points inside the domain using the above first order accurate space derivatives. Boundary conditions like no slip boundary, inflow and outflow boundary etc. are implemented wherever applicable in this step.

Step 11: This step is required for implementing second order accuracy. If some nodes exist inside the flow domain where second order accuracy of the space derivatives are required then for those nodes, second order accurate space derivatives of the inviscid and viscous fluxes are calculated and values of the field variables are updated using those derivatives.

Step 12: Residue based on value of a field variable at previous and current time level is computed in this step. If \mathfrak{N}_i^n is the value of a field variable at iteration n at any node i, and \mathfrak{N}_i^{n+1} is its value at iteration n+1 at the same node then residual

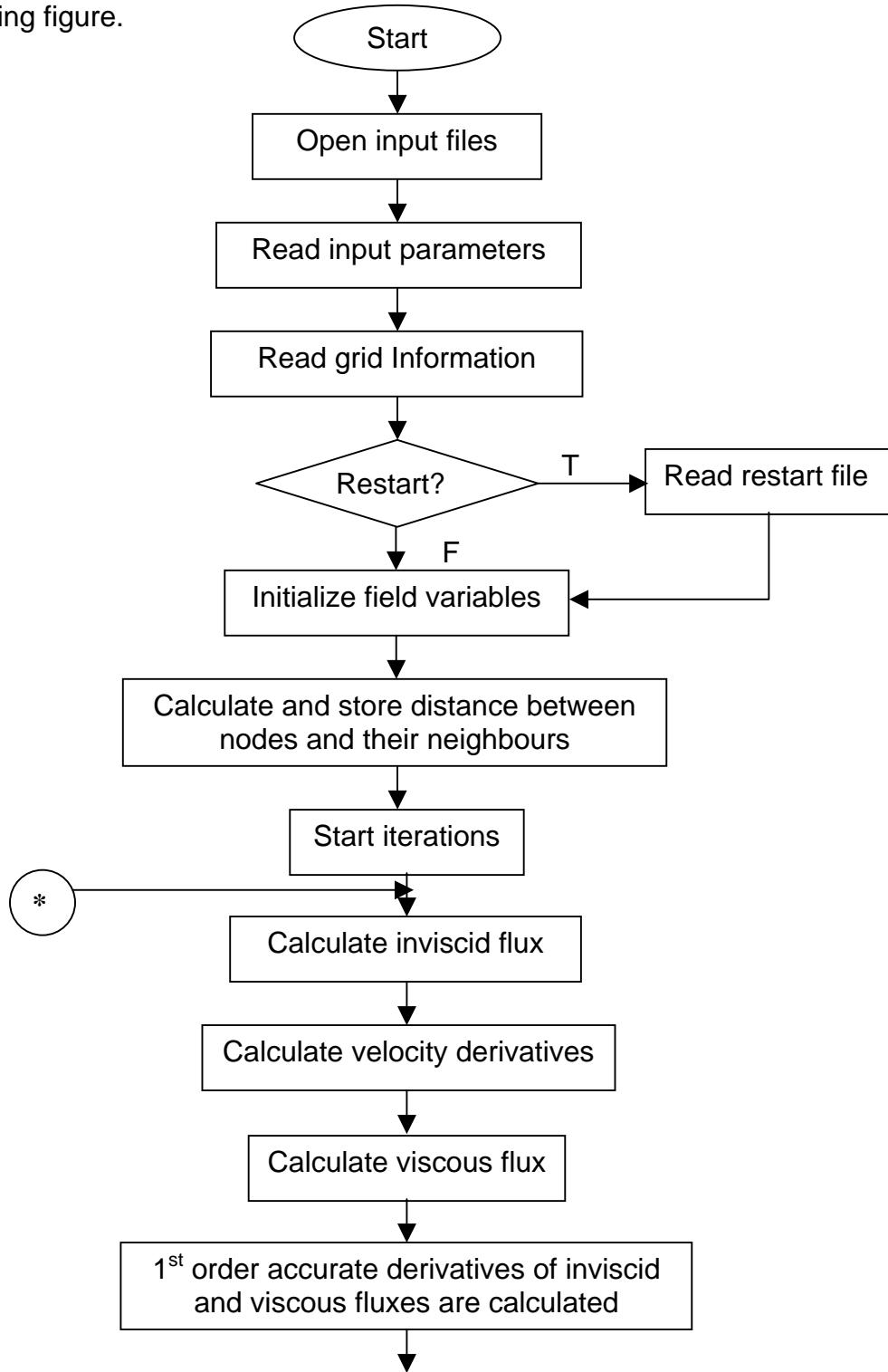
$$\mathfrak{R} = \max_i |\mathfrak{N}_i^{n+1} - \mathfrak{N}_i^n| \quad (3.10)$$

Step 13: Latest output data file and restart data file are created. The output data file stores the data in a format that can readily be used for post processing and visualization

Step 14: Steps 6 to 13 are repeated for given number of iterations and value of the residue is observed. When residual converges the looping can be terminated and the latest output data file becomes the final data file.

3.5 Schematic of code

The steps of the artificial compressibility code are described by the following figure.



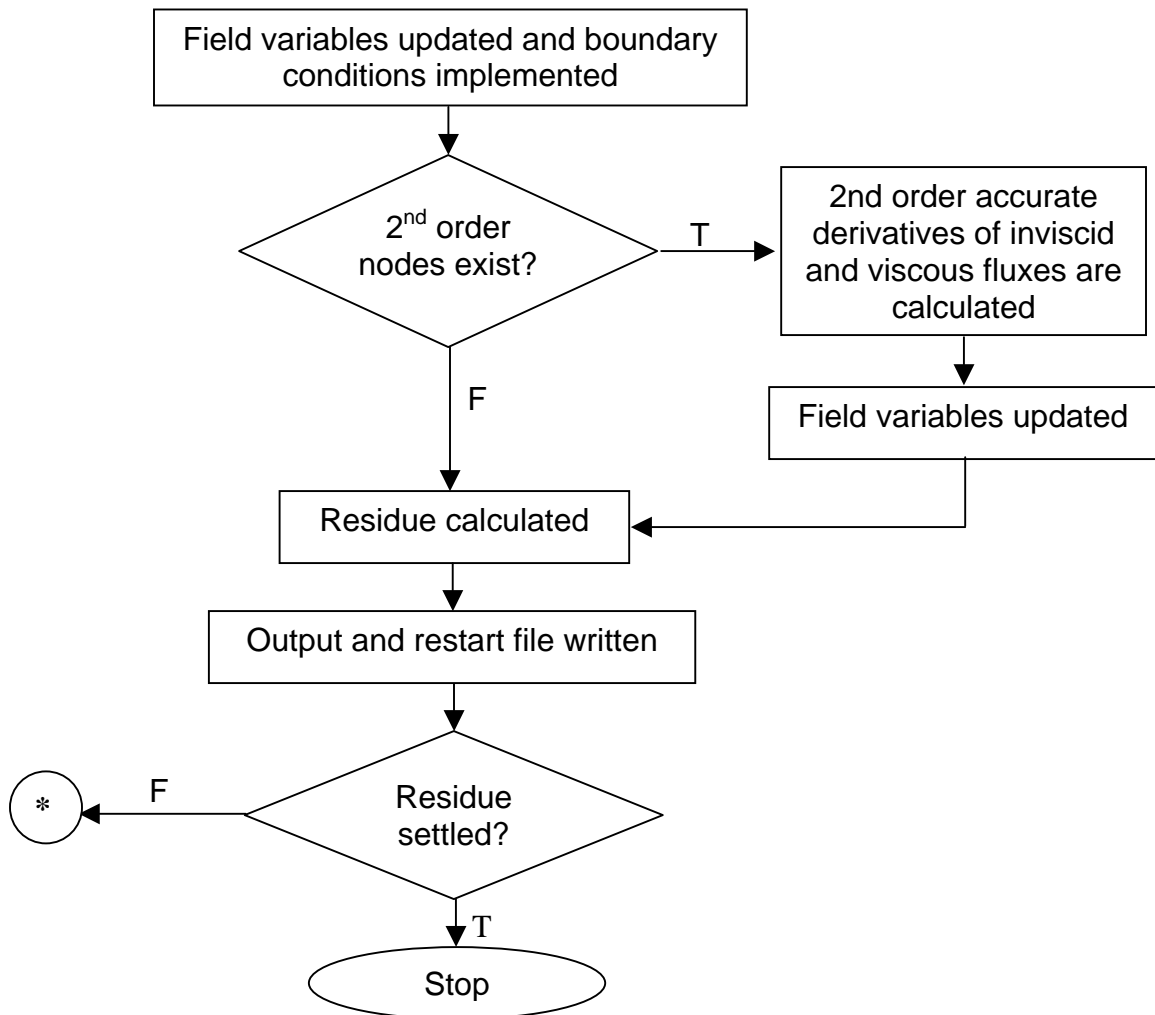


Figure 3.3: Schematic of the code developed

3.6 Summary

In this chapter meshless code development has been discussed. Initially a literature survey on the meshless method has been presented followed by a description of least square based discretisation technique. Next how upwinding is enforced in least square based discretization method by stencil subdivision has been described. Finally detailed features of the code have been described.

CHAPTER 4

Code Validation

4.0 Introduction

In this chapter the two-dimensional incompressible meshless solver based on artificial compressibility method has been validated with following test cases.

1. Fully developed flow between two parallel plates
2. External flow over a flat plate (Blasius Solution)
3. Flow inside a lid driven cavity
4. Flow past a circular cylinder
5. Flow over a backward facing step
6. Laminar axisymmetric sudden expansion flow

4.1 Fully developed flow between two parallel plates

In this test case, we apply the scheme to a Poiseuille flow in a section of length L between two parallel plates of infinite length (in x -direction) at a distance d . The system of equations (2.8-2.10) is solved in a domain D : $0 \leq x \leq L$, $-d/2 \leq y \leq d/2$ (refer to figure 4.1a), with the boundary conditions

$$u_1 = u_{\max} \left[1 - \left(\frac{y}{d/2} \right)^2 \right], u_2 = 0 \text{ at the boundary } x=0, x=L$$
$$u_1 = u_2 = 0 \text{ at the boundary } y = -d/2, y = +d/2,$$
$$\frac{\partial p}{\partial y} = 0 \text{ at } y = -d/2, y = +d/2 \quad (4.1)$$

This is a simple problem, designed to test our method. The domain D

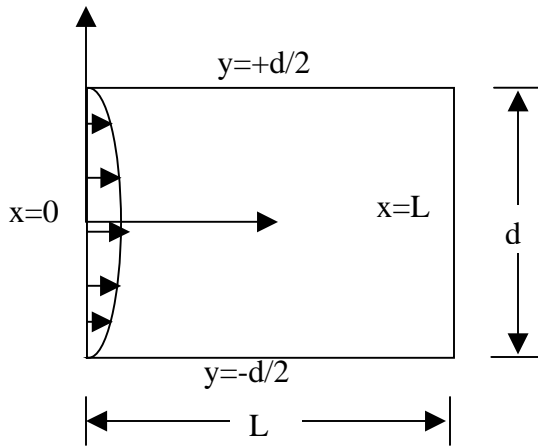


Figure 4.1a Computational domain

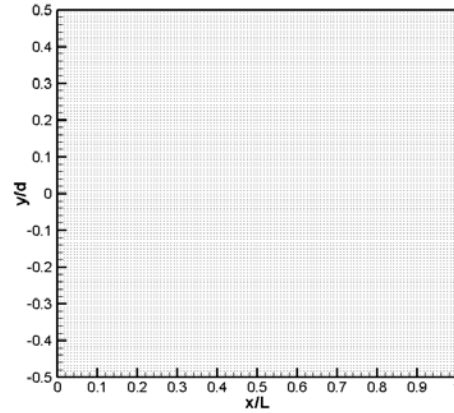


Figure 4.1b Grid for flow between parallel plates

represents a segment between two parallel plates. The reference velocity in the Reynolds number is the maximum velocity (u_{max}) inside the parallel plates, and the reference length d is the distance between the plates in y direction. The unstructured grid used for computation is shown in figure 4.1b. Analytical solution for fully developed flow is given by

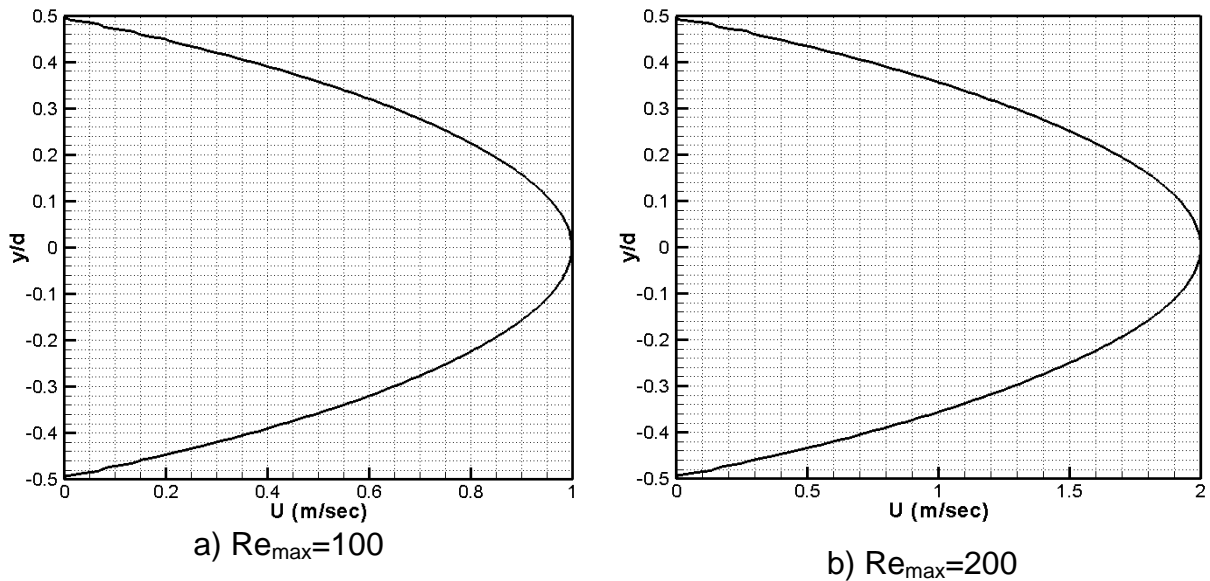
$$u_1(y) = u_{max} \left[1 - \left(\frac{y}{d/2} \right)^2 \right], u_2 = 0, u_{max} = \frac{\Delta P d^2}{16\mu L} \quad (4.2)$$

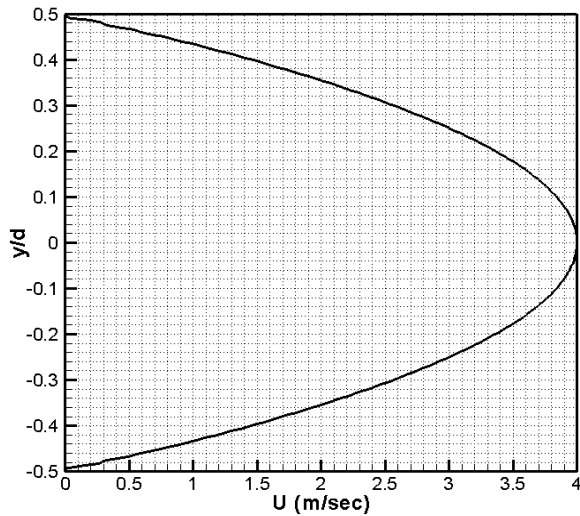
where, $\Delta p = p_1 - p_2$

The pressure p_1 at the left boundary of the domain is higher than the pressure p_2 at the right boundary of the domain. The flow profile is parabolic in nature. The initial values for equation (2.8-2.10) or the initial guess for the steady solution are very unfavorable: $u_1 = u_2 = 0$ everywhere except at the boundary, $p=0$ everywhere. These initial values are very unfavorable because u_1 is discontinuous. These initial values were chosen to demonstrate the convergence of the procedure even under unfavorable conditions. The optimal value of artificial compressibility parameter, δ_{opt} has been determined from a preliminary test computation so that the stability requirement is met. δ_{opt} is not sharply defined. The value of the time step is determined from the relation

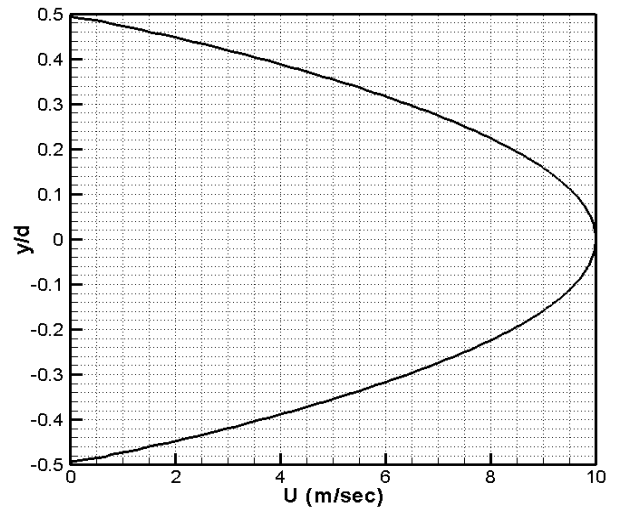
$$\Delta t = 0.6 \Delta x \delta^{-1/2} \quad (4.3)$$

The above flow problem is solved for different values of maximum Reynolds number (based on local u component of velocity and the characteristics dimension) varying between 100 and 1000. The aim of the simulation is to capture the parabolic velocity profile for a fixed pressure drop along the length. The distance between the plates in the y direction and the density of the fluid is taken as unity while the viscosity of the fluid is taken as 0.01. The method converged for all these values, although convergence is very slow for the higher values of Reynolds number. δ_{opt} decreases as Reynolds number increases. Figure 4.2 displays the variation of u component of velocity along the cross section of the flow area for values of maximum Reynolds number varying between 100 and 2000. Figure 4.2 also shows the residue plot with iterations in pseudo time. The residue is calculated at each pseudo time step using the l_∞ norm given by equation (3.10).

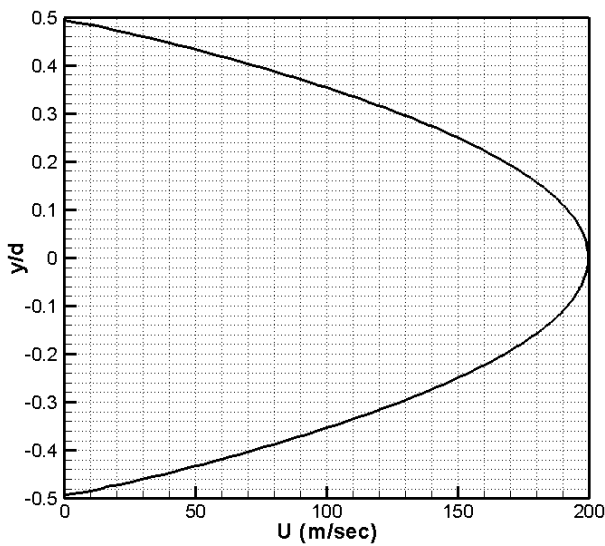




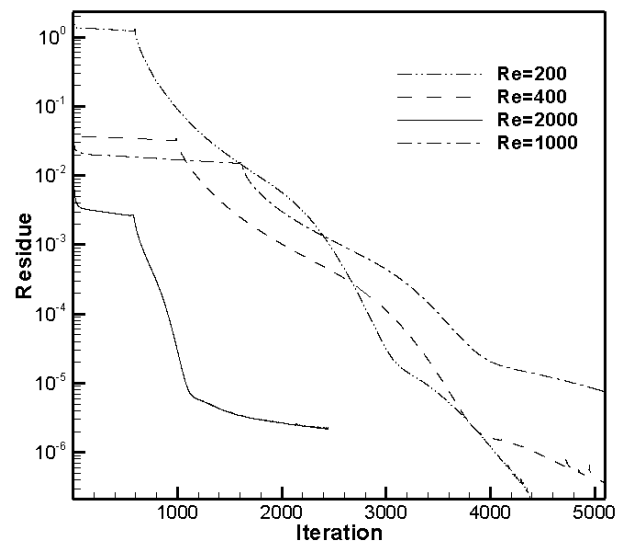
c) $Re_{max}=400$



d) $Re_{max}=1000$



e) $Re_{max}=2000$



f) Residue plot

Figure 4.2 Reynolds number contours and residue plot for flow between parallel plates

4.2 Isothermal laminar Flow

In this category two benchmark problems have been solved.

- External flow over a flat plate
- Flow inside a lid driven square cavity

4.2.1 External flow over a flat plate (Blasius solution)

Blasius in 1908 first treated the incompressible steady flow over a flat plate as an explicit solution of the Prandtl equations. The classical problem

Blasius considered, was a two-dimensional steady, incompressible flow over a flat plate at zero angle of incidence with respect to the uniform incoming stream of velocity u_α . The fluid extends to infinity in all directions from the plate. The physical problem is shown in figure 4.3.



Figure 4.3 External flow over a flat plate

Using ACM the modified Navier-Stokes equations (2.8- 2.10) has been solved over a flat plate at Reynolds number 10,000. For this problem an adapted unstructured grid has been used. The grid has been made highly clustered near the flat plate and adapted based on velocity gradient as shown in figure 4.4 in order to capture the boundary layer. The plate starts at $x=0.5$. At the entry length ($x=0.0$ to $x=0.5$) symmetry boundary condition is maintained. This entry length helps in capturing an undisturbed boundary layer over the flat plate free from any disturbance at the inlet.

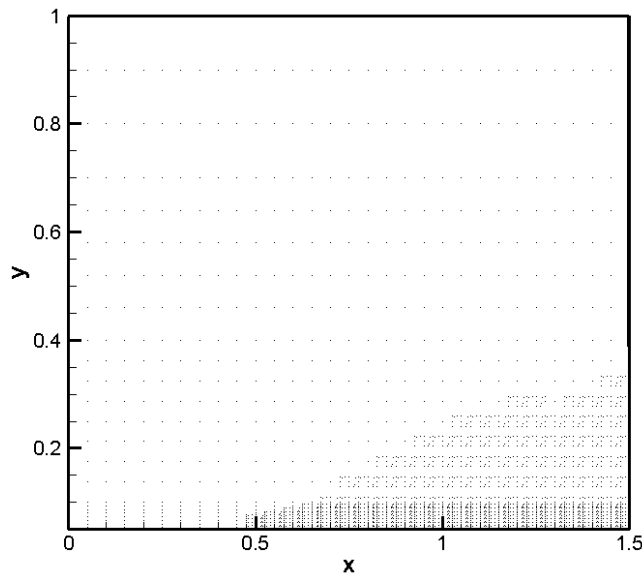


Figure 4.4 Grid used for Blasius problem

The following boundary conditions have been used for the flow simulation.

- No slip boundary condition on the flat plate surface ($y=0$ and $x=0.5$ to 1.5).
- Symmetry boundary condition has been maintained at the zone $x=0.0$ to 0.5 . This treatment of the boundary condition corresponds to the physical assumption that, on the two sides of a node, the same physical processes exist. The variable values at the same distance from the boundary at the two sides are the same. The function of such a boundary is that of a mirror that can reflect all the fluctuations generated by the simulation region.

Assume $f(x_b)$, $f(x_b - \Delta x)$ are two adjacent boundary values,

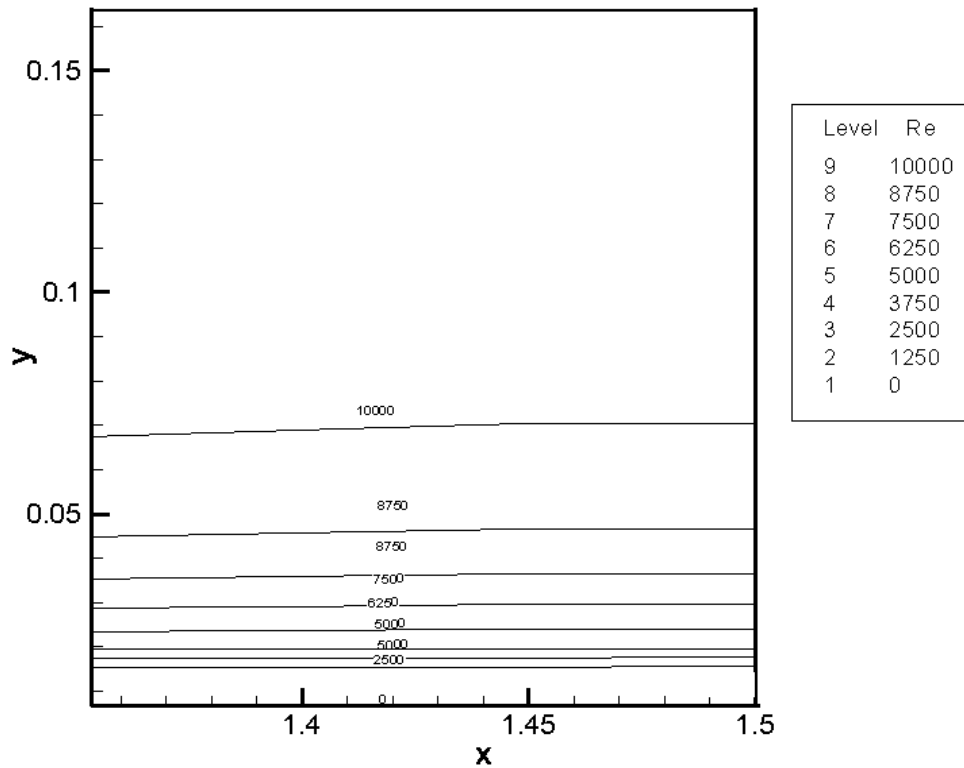


Figure 4.5 Reynolds number contour

a typical set of symmetric boundary value is

$$f(x_b + \Delta x) = f(x_b) \quad (4.4)$$

$$f(x_b + 2\Delta x) = f(x_b - \Delta x) \quad (4.5)$$

- Uniform velocity $u = u_\alpha$ has been maintained at the inlet ($x=0.0$).
- Static pressure is kept constant at the exit ($x=1.5$).

Figure 4.5 shows the Reynolds number contour near the flow exit, computed through the ACM based meshless code developed. The plot of $y\sqrt{\frac{u_\infty}{\nu x}}$

vs. $\frac{u}{u_\infty}$ for the axial location $x=1.48$ are shown in figure 4.6a. These are matching well with the Blasius solution plotted in the same figure as obtained from Yuan (1969). It can be seen from the plot that the line asymptotically converges to the value one as for the case of Blasius. Figure 4.6b gives the residue plot for the same problem.

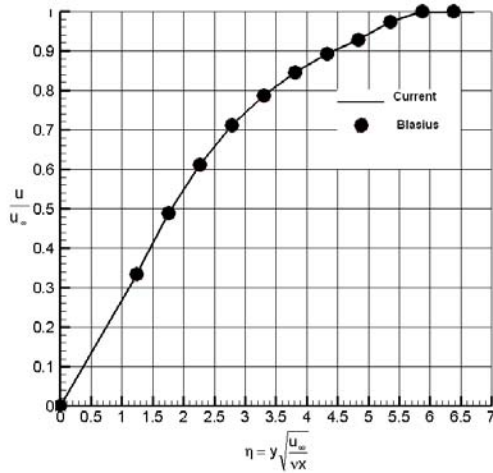


Figure 4.6a Present and Blasius solution for flow over flat plate

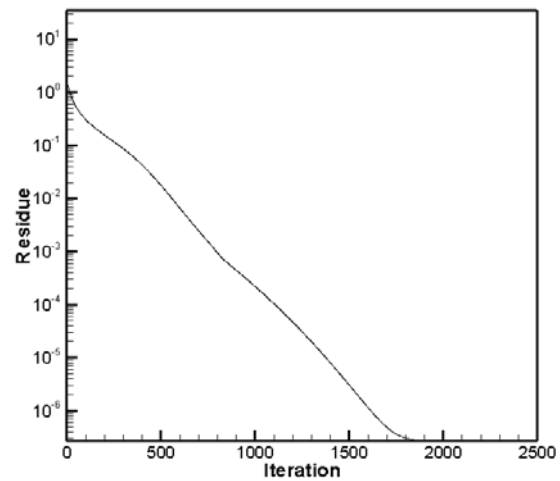


Figure 4.6b Residue plot for flow over flat plate

4.2.2 Flow inside a lid driven cavity

The two-dimensional laminar incompressible flow in a lid driven square cavity of unit length whose top wall moves with a uniform velocity u in its own plane has been used rather extensively as a validation test case by many authors in the recent past. It has served as a benchmark problem for testing and evaluating numerical techniques for different Reynolds number. It provides a

good test case in that there is no primary flow direction and the boundary conditions are very simple to employ. Ghia et. al. (1982) presented extensive numerical study obtained from their multigrid vorticity–stream function formulation using very fine grids. They reported results, which agreed quite well with other computational efforts. Other recent computational work involving this particular geometry includes Schreiber and Keller (1983) who have used a vorticity-stream function formulation; Kim and Moin (1985) who have used a fractional-step method in primitive variables in conjunction with approximate factorization; Vanka (1986) who has used a multigrid technique in primitive variables; and Benjamin and Denny (1979) who have used a centrally differenced vorticity-stream function formulation in conjunction with an ADI scheme.

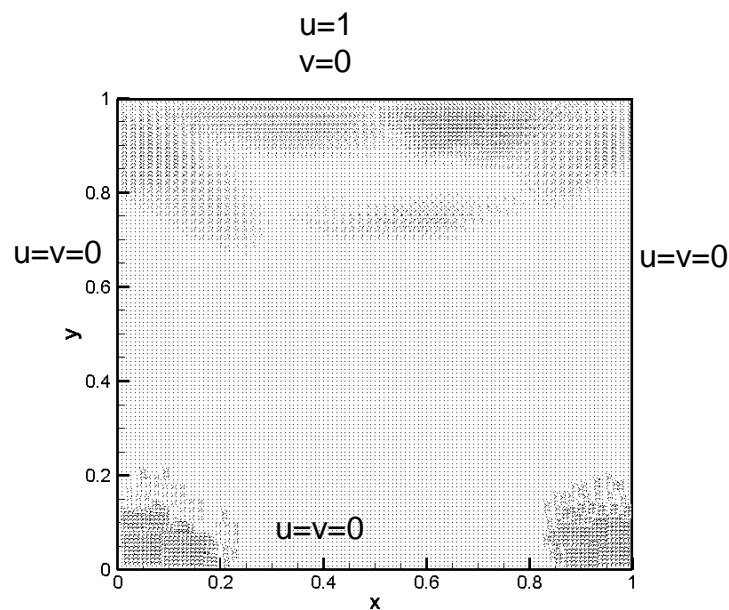
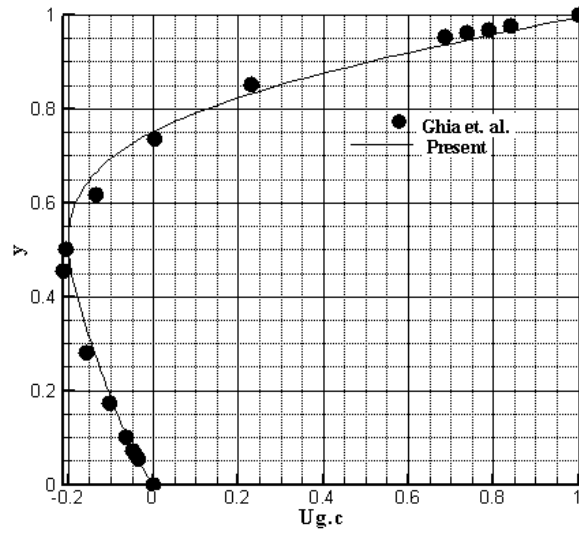
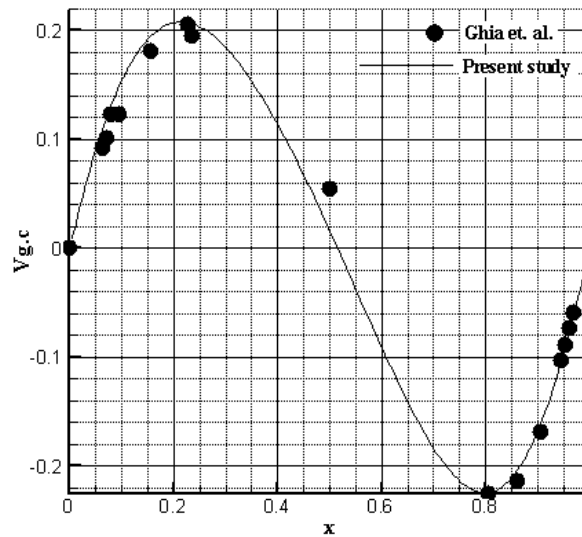


Fig 4.7 Lid-driven cavity problem; nodes with boundary conditions

The current code has been validated for lower range of Reynolds number, i.e. $Re=100$, $Re=400$ and $Re=1000$. For Reynolds number 100, 400 and 1000, the value of the artificial compressibility δ was set to 2.0, 1.0 and 0.5 respectively. The top lid has been specified at horizontal speed of unity while no slip boundary condition has been applied for other walls. In all the four boundaries normal pressure gradient is equated to zero. Figure 4.7 shows a domain with 14641 nodes used for this problem.



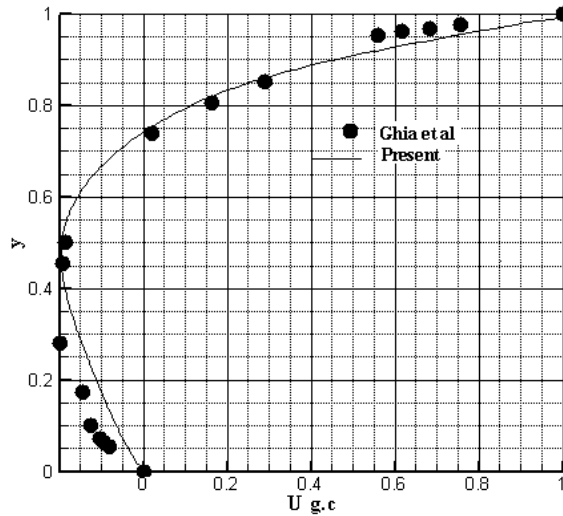
a) u-velocity distribution at $x=0.5$



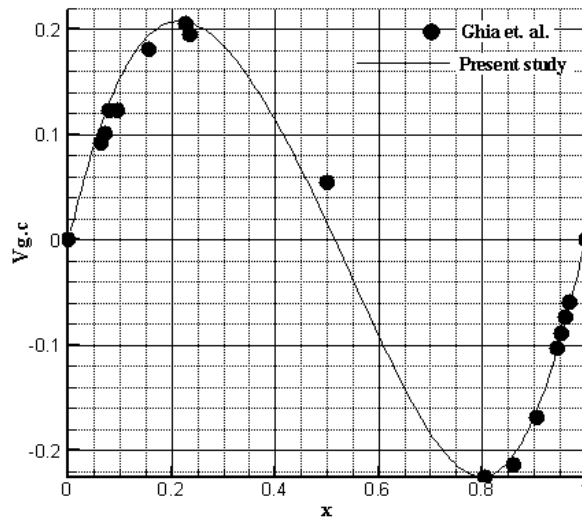
b) v-velocity distribution at $y=0.5$

Figure 4.8 Predicted velocity distribution for the lid driven cavity problem at $Re=100$

The velocity components on the lines passing through the geometric center of the cavity are compared to the results of Ghia et al. (1982). For quantitative validation, the horizontal velocity component ($u_{g.c}$) along the vertical mid plane of the cavity and the vertical velocity component ($v_{g.c}$) along the



a) u-velocity distribution at x=0.5



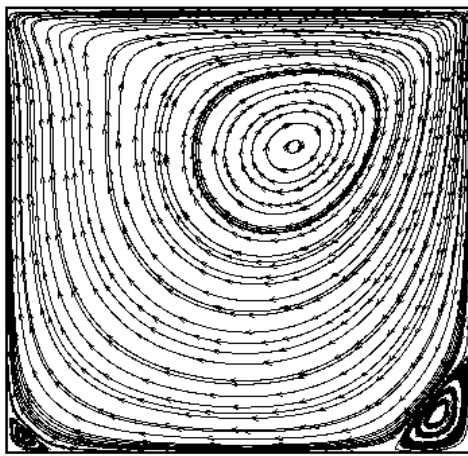
b) v-velocity distribution at y=0.5

Figure 4.9 Predicted velocity distribution for the lid driven cavity problem at $Re=400$

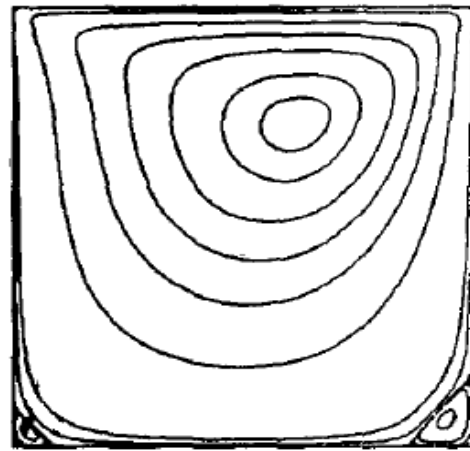
horizontal mid plane of the cavity are compared against the standard benchmark solution of Ghia et al. (1982), for Reynolds Number = 100, 400 and 1000. The results are given below.

Figure 4.8 shows the velocity plots for Reynolds number = 100. Here we see that the computed values match well with the reference values. Figure 4.9 shows results for higher Reynolds number of 400. Here also there is good agreement with the reference values. Both the plot of u and v component of

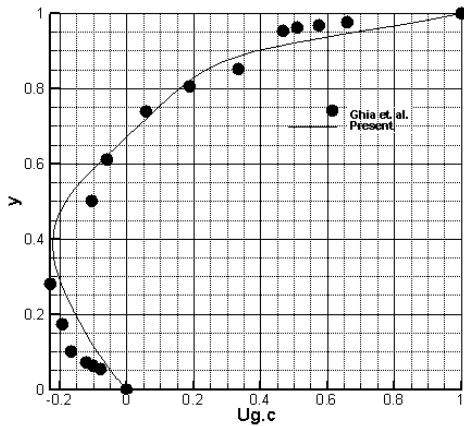
velocity along the geometric center of the cavity for a flow with Reynolds number of 400 show good match with the benchmark result. The result for flow with Reynolds number = 1000 is shown in figure 4.10. Comparing the results with those of the benchmark paper on driven cavity it has been observed that in this case also a good agreement between the result obtained by present code and that reported by the benchmark paper has been obtained.



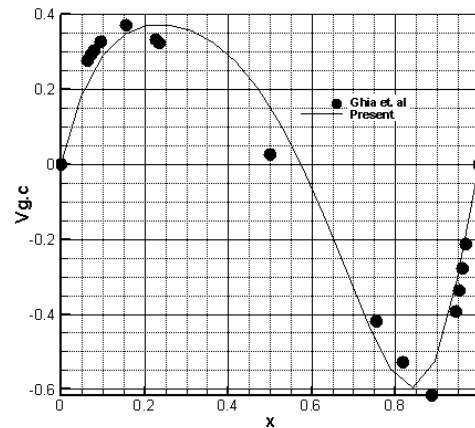
a) Stream line plot (present code)



b) Stream line plot from Ghia et. al.



c) u-velocity distribution at x=0.5



d) v-velocity distribution at y=0.5

Figure 4.10 Predicted Stream line plot and velocity distribution for the lid driven cavity problem at Re=1000

4.3 Flow past a circular cylinder

The capabilities of the present method are demonstrated by simulating the laminar flow over a circular cylinder. This flow has been computed extensively and used as a benchmark to examine the accuracy of new numerical methods for a long time. It is well-known that the flow exhibits vastly different patterns as the Reynolds number $Re = \frac{U_\infty D}{\nu}$ changes, where U_∞ is the free-stream velocity, D is the cylinder diameter, and ν is the kinematic viscosity. The total length of the grid is taken as $38D$. The cylinder is placed at a distance of $8D$ from the left boundary, midway from the top and bottom boundary (i.e. at $16D$). At small Reynolds numbers, i.e., from zero up to approximately $Re_{critical} \cong 49$ (Ding, (2004)), the flow maintains a stable pattern with a pair of symmetric counter-rotating vortices behind the cylinder. In the present study, we performed numerical simulation at a series of Reynolds number from 10 to 40 with various flow patterns in the steady state.

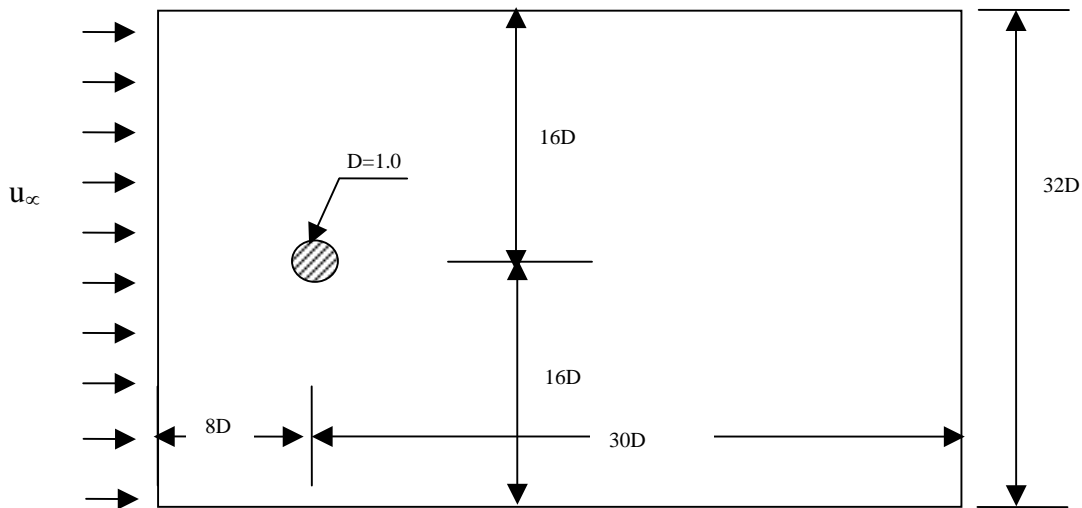


Figure 4.11 Configuration of flow past a circular cylinder

To solve the governing equations for the flow around a circular cylinder in an infinite fluid domain, boundary conditions have to be specified over the body surface and at infinity. No-slip condition is imposed over the body surface and the

free stream condition away from the cylinder. The mathematical representation of these boundary conditions is presented below in equations (4.4 to 4.6).

On the body:

$$\begin{cases} u = 0 \\ v = 0 \\ \frac{\partial p}{\partial n} = 0 \end{cases} \quad (4.4)$$

At infinity and inflow:

$$\begin{cases} u = U_{\infty} \\ v = 0 \end{cases} \quad (4.5)$$

At outflow:

$$\begin{cases} u = \text{outflow} \\ v = \text{outflow} \end{cases} \quad (4.6)$$

Pressure is updated at the inflow and infinity boundary while specified at the outflow. The numerical solution of the governing equations requires the specification of an initial condition in order to start the time-marching method. In the present work, the free stream characteristics are applied everywhere as initial conditions. Equation (4.7) below shows the mathematical representation of these conditions.

$$\begin{cases} u = U_{\infty} \\ v = 0 \\ p = 1 \end{cases} \quad (4.7)$$

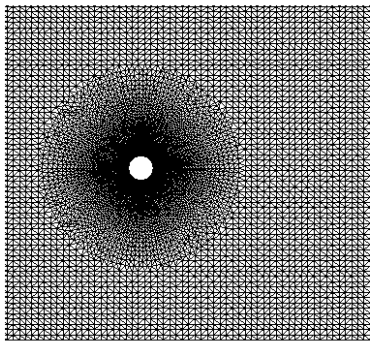


Figure 4.12 Composite grid

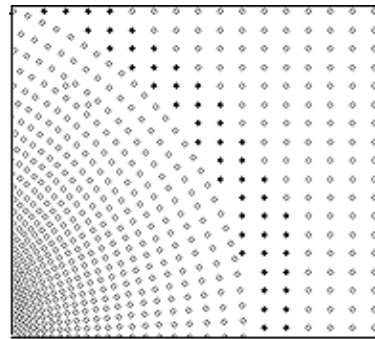


Figure 4.13 Detailed grid structure

A special composite mesh is designed to exploit the performance of the present method. In the composite mesh, Cartesian nodes are generated as the background mesh, and the nodes around the solid body are generated with the consideration of the geometrical description to make the meshing easier. A typical example of the composite mesh generated near the cylindrical body is shown in Figure 4.12.

A detailed local pattern of node distribution is demonstrated in figure 4.13, which shows the background Cartesian nodes and the nodes around the solid body. In principle, the concept of mesh-free least square-based discretization works well for any “mesh” system, in which the nodes can be either regularly or irregularly distributed. This makes the present meshless method acquire geometric flexibility. However for simplicity and convenience, the nodes in the neighbourhood of the circular cylinder are generated under the cylindrical coordinate system. Beyond this neighbourhood, Cartesian mesh is appropriately generated. For meshless method no special treatment of the interface between the two meshes is required and it can be of any shape, depending on the convenience and requirement of the user.

Numerical simulations were carried out for flow past circular cylinder for small Reynolds numbers of: 20, 30 and 40 respectively. Figures 4.14a, 4.14b and 4.14c illustrate the velocity contour and streamlines when flow reaches its final steady state for three different Reynolds numbers of 20, 30 and 40 respectively. The corresponding fall in residue is also plotted with the iterations in those figures. In all cases, a pair of vortices develops behind the cylinder. It is also observed from the numerical solution that ripples are present behind the vortices inside the disturbed zone.

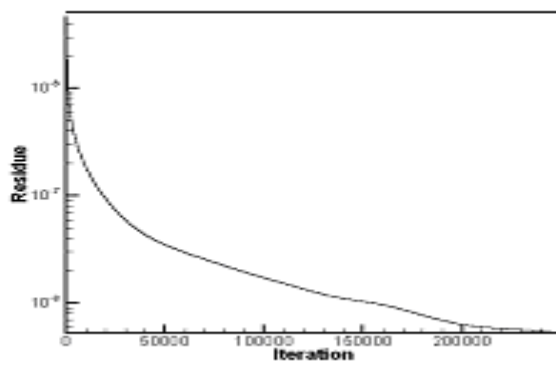
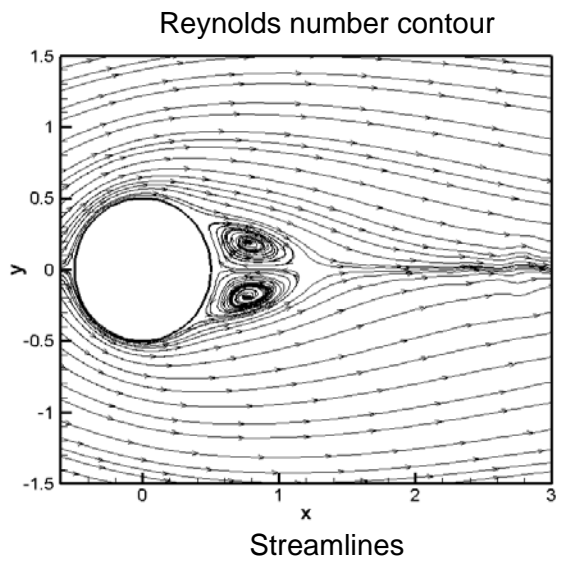
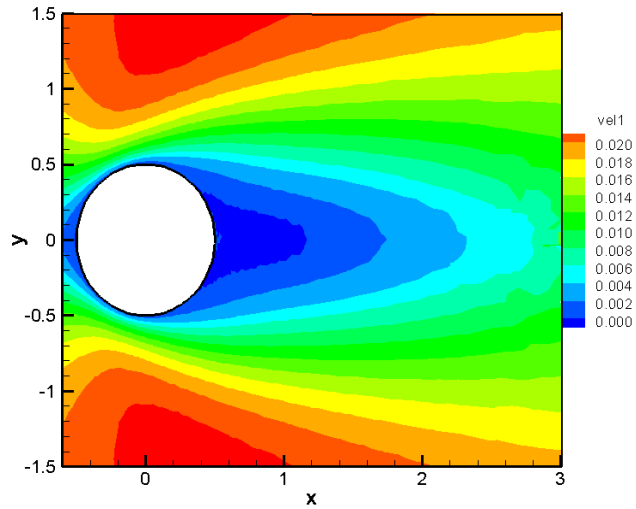


Figure 4.14a: Reynolds number contour, streamline and residual plot for flow past circular cylinder at Reynolds number=20.

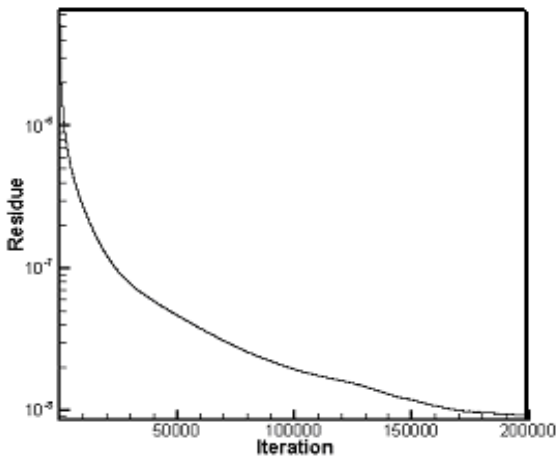
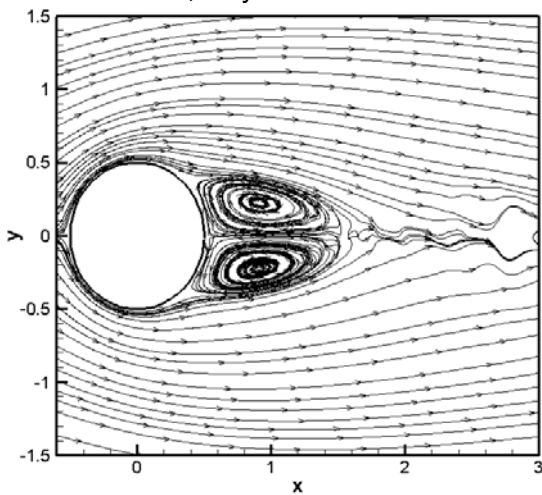
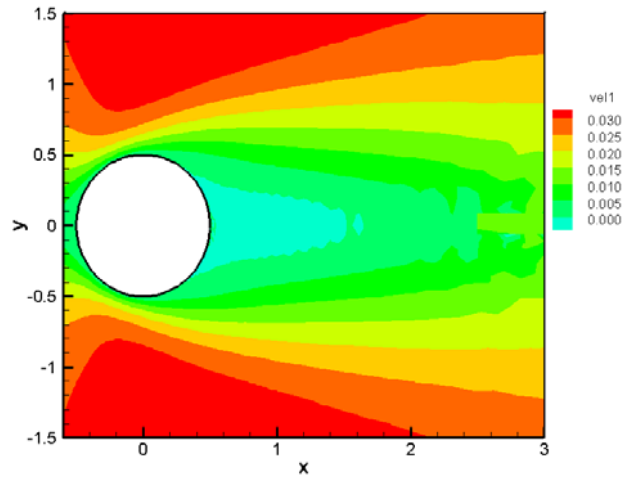
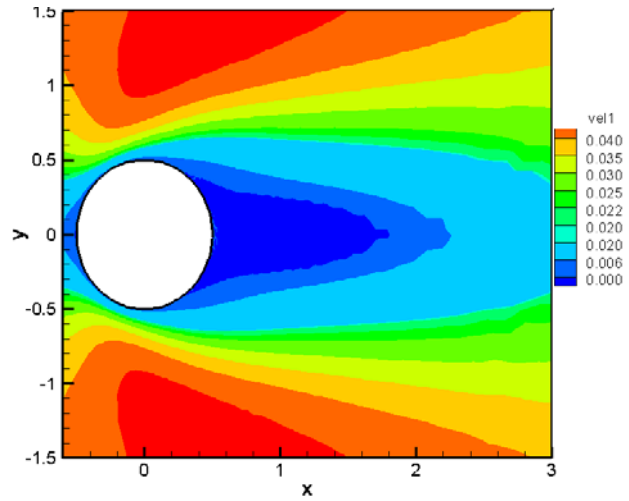
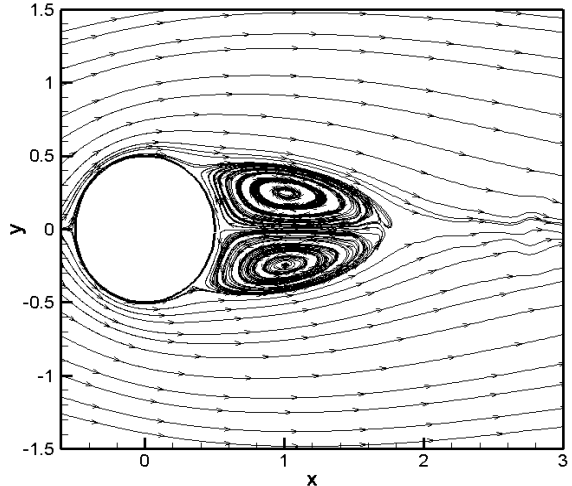


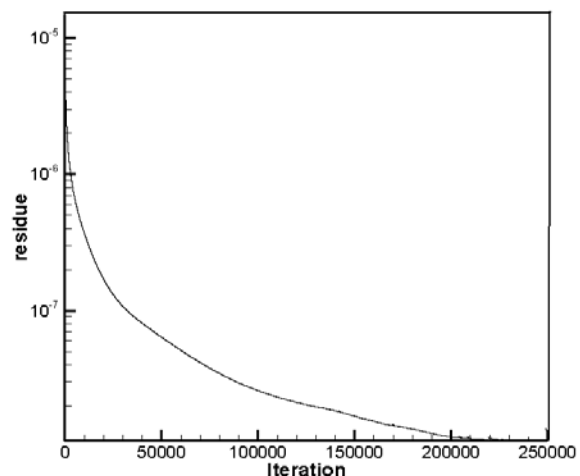
Figure 4.14b: Reynolds number contour, streamline and residual plot for flow past circular cylinder at Reynolds number=30.



Re= 40; Reynolds number contour



Re=40;Streamlines



Re=40;Residue

Figure 4.14c: Reynolds number contour, streamline and residual plot for flow past circular cylinder at Reynolds number=40.

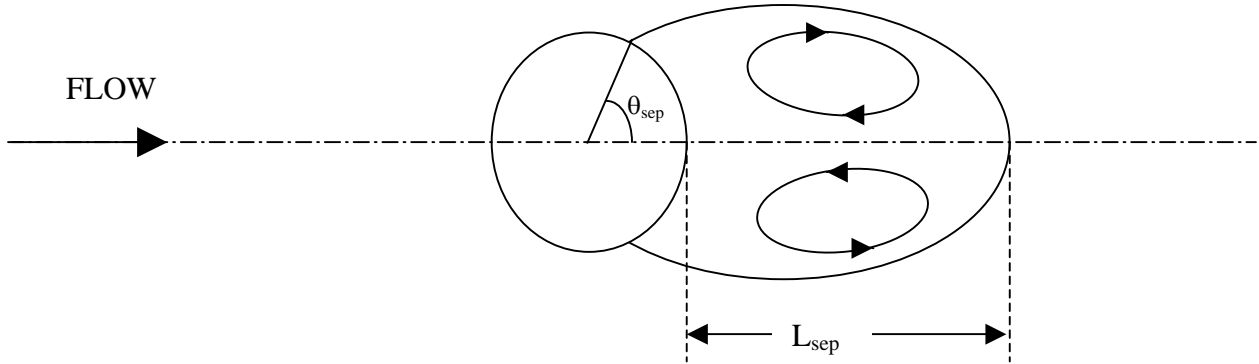


Figure 4.15: Characteristic parameters of the cylinder's wake

For the fluid flow past a circular cylinder, the characteristic quantities usually include the wake length L_{sep} , the separation angle θ_{sep} and the drag coefficient C_d . The wake length, L_{sep} , is defined as the distance from the rear of the cylinder to the end of the separated region. The separation angle, θ_{sep} , is determined from zero-vorticity at the surface of the cylinder, where the vorticity ω can be calculated from the following equation

$$\omega = \frac{\partial v}{\partial x} - \frac{\partial u}{\partial y} \quad (4.8)$$

The drag coefficient C_d is computed by

$$C_d = \frac{F_D}{\frac{1}{2}\rho u_\infty^2 A} \quad (4.9)$$

where F_D is drag force, ρ the characteristic fluid density, A is area of the orthogonal projection of the cylinder on a plane perpendicular to the direction of motion. The drag force on the circular cylinder can be expressed as (Zhang et. al. (2005))

$$F_D = \oint_s -p \cos \phi ds + \oint_s \tau \sin \phi ds \quad (4.10)$$

where p is the pressure along the cylinder surface, τ the shear force on the cylinder surface, ϕ is the angle between the normal to the surface element and the flow direction, s the total surface area of the circular cylinder. The results from the present calculation as well as the result of the other researchers, Dennis (1970), Takami (1969), Tuann(1978), Fornberg (1980), Ding (2004), are listed in Table 4.1 for the test case of Reynolds number of 20 and 40. All these flow parameters agree well with the results of previous studies for the range of Reynolds number studied.

Table 4.1: Comparison of length of re-circulating region (L_{sep}), separation angle (θ_{sep}) and drag coefficient (C_d) for $Re= 20$ and 40

Re	Source	L_{sep}	θ_{sep}	C_d
20	Dennis et. al. (1970)	0.94	43.7	2.05
	Takami et. al. (1969)	0.935	43.7	2.05
	Tuann et. al. (1978)	0.9	44.1	2.25
	Fornberg et al. (1980)	0.91	-	2.00
	Ding et. al. (2004)	0.93	44.1	2.18
	Present	0.94	43.7	2.08
40	Dennis et. al. (1970)	2.35	53.8	1.522
	Takami et. al. (1969)	2.32	53.6	1.536
	Tuann et. al. (1978)	2.1	54.8	1.675
	Fornberg et al. (1980)	2.24	-	1.498
	Ding et. al. (2004)	2.20	53.5	1.713
	Present	2.11	54.4	1.795

4.4 Flow over a backward facing step

Fluid flows in channels with flow separation and reattachment of the boundary layers are encountered in many flow problems like heat exchangers and ducts. Among this type of flow problems a backward facing step can be regarded as having a simple geometry while retaining rich flow physics manifested by flow separation, flow reattachment and multiple recirculating zones

in the channel depending on the Reynolds number, and the geometrical parameters like step height and channel height. This problem has been used as

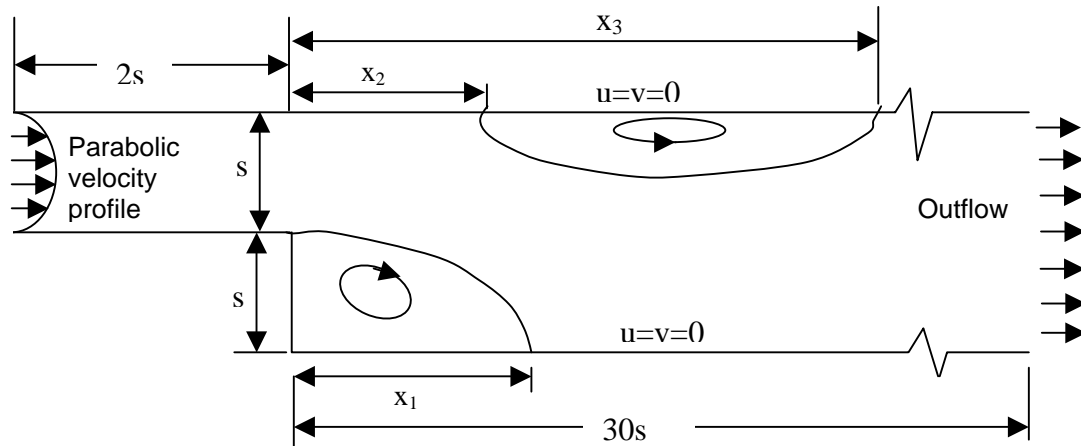


Figure 4.16: Outline of the backward facing step problem

a validation case. The challenge in modeling this problem comes from the fact that the sizes of the separation zones downstream of the step are very sensitive to the pressure gradient in the flow, especially when the boundary layer is separated. If separation is present, a pressure wave traveling with finite speed will cause a change in the local pressure gradient, which will affect the location of the flow separation. It has been observed that this change in separated flow will cause a feed back to the pressure field, possibly preventing convergence to a steady state. The geometry used in the calculation is shown in figure 4.16, where s is the height of the step. The entrance channel width is equal to the step height and its length is double the step height. The total length of the channel from the step is $30s$. The length of the primary circulation zone behind the step is denoted by x_1 , whereas the distance of the starting and end point of the secondary circulation zone are x_2 and x_3 respectively.

In the literature, a rich amount of numerical studies can be found on the two-dimensional steady incompressible flow over a backward facing step like Guj and Stella (1988), Keskar and Lyn (1999), Barton (1998), Kim and Menon (1999).

Rogers and Kwak (1987) applied an upwind differencing scheme in conjunction with the artificial compressibility method for the incompressible Navier-Stokes equations and have taken flow over a backward facing step as an example problem. While the flow over a backward-facing step serve as an interesting benchmark flow problem for many numerical studies, some studies stated that the inlet and exit boundary condition used for the model problem can affect the numerical solution. Barton (1998) studied the entrance effect for flow over a backward facing step. He stated that when using an inlet channel upstream of the step, significant differences occur for low Reynolds numbers, however, they are localized in the sudden expansion region. Papanastasiou et al. (1992) studied the effect of the outflow boundary condition on the numerical solution in a backward facing step flow. Gartling (1990) stated the importance of the outflow boundary condition for the considered flow. Erturk (2008) suggested that not only the inlet channel and outflow boundary condition that can affect the numerical solution inside the computational domain but the location of the outflow boundary is also very important for the accuracy of the numerical solution.

In a very important study Yee et al. (1999) observed the spurious behavior of the numerical schemes. They showed that for backward facing step flow when a coarse grid mesh is used, one can obtain a spurious oscillating numerical solution. Yee (1999) and Erturk (2008) have reported that when a finer grid mesh was used, the oscillating behavior of the numerical solution disappeared and it was possible to obtain a steady solution. They stated that when finer grids are used, the Mesh Reynolds number defined as $Re_m = \frac{u\Delta h}{\nu}$ decreases and this

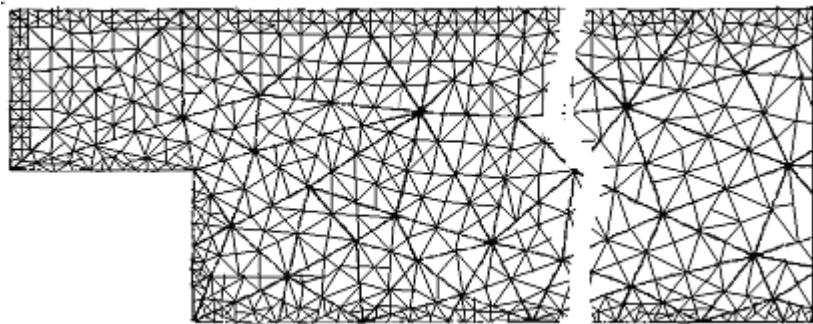
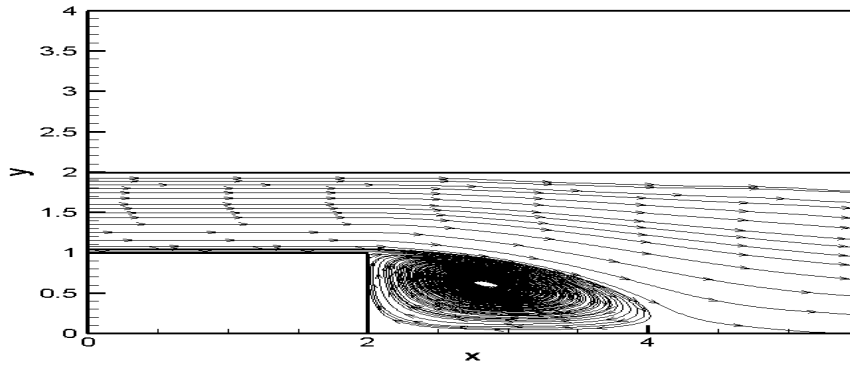


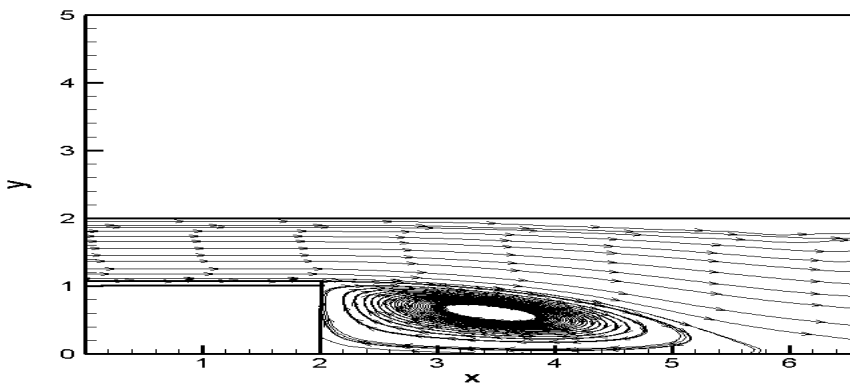
Figure 4.17: Grid used for computation of flow over backward facing step

improves the numerical stability characteristics of the numerical scheme used, and allows high Reynolds number flows computable. In the present study, following Yee et al. (1999) and Erturk et al. (2008), a fine unstructured mesh is used in order to be able to obtain steady state numerical solutions. A part of the grid used for computation is shown in figure 4.17.

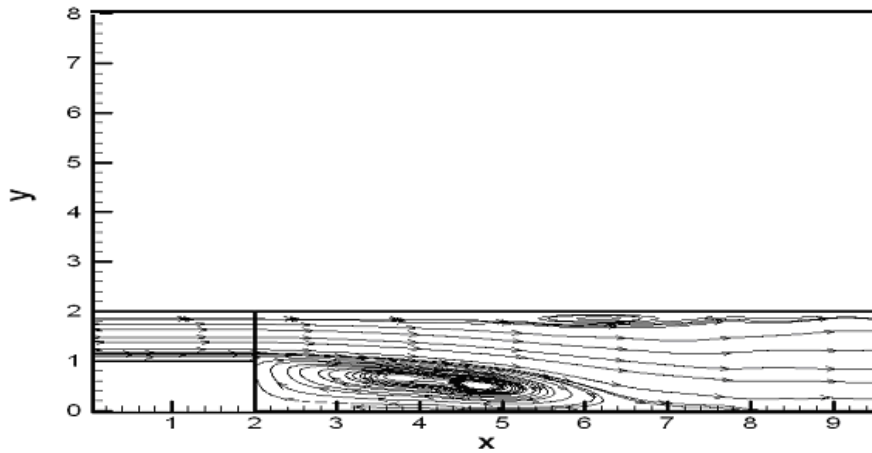
At the inflow boundary, it is assumed that the flow is fully developed plane Poiseuille flow between parallel plates such that a parabolic velocity profile is prescribed throughout the calculation, and the static pressure is allowed to change. No slip boundary condition is prescribed at the top and bottom wall. Two step heights downstream from the inflow a two to one expansion is encountered. The outflow boundary extends to 30 step heights downstream of the step. At this exit boundary an outflow boundary condition has been used such that any wave generated in the computation domain could pass through the exit boundary and leave without any reflection back into the computational domain. The ability of the code to predict the reattachment length x_1 , of the primary separation zone behind the step, as well as the separation and reattachment locations, x_2 , and x_3 , of the secondary separation zone on the opposite wall was tested by comparing the computed result to that available in published literature. These quantities were measured for laminar range of Reynolds numbers, which are based on the average inflow velocity and twice the step height. The flow was calculated using a grid of 24600 points. The grid is unstructured and clustered near the side boundary for better resolution of the flow features to be captured. The initial conditions were specified to be free-stream velocity at the interior points with uniform pressure everywhere. The streamline plot for different Reynolds number is shown in figure 4.18. It is observed from the plots that as the Reynolds number increases the length of the primary separation zone x_1 also increases. At Reynolds number = 400 a secondary separation zone has been developed at the top wall boundary.



a) Entry Reynolds number = 100



b) Entry Reynolds number = 200



c) Entry Reynolds number = 400

Figure 4.18: Streamline plot for flow over a backward facing step at different Reynolds number

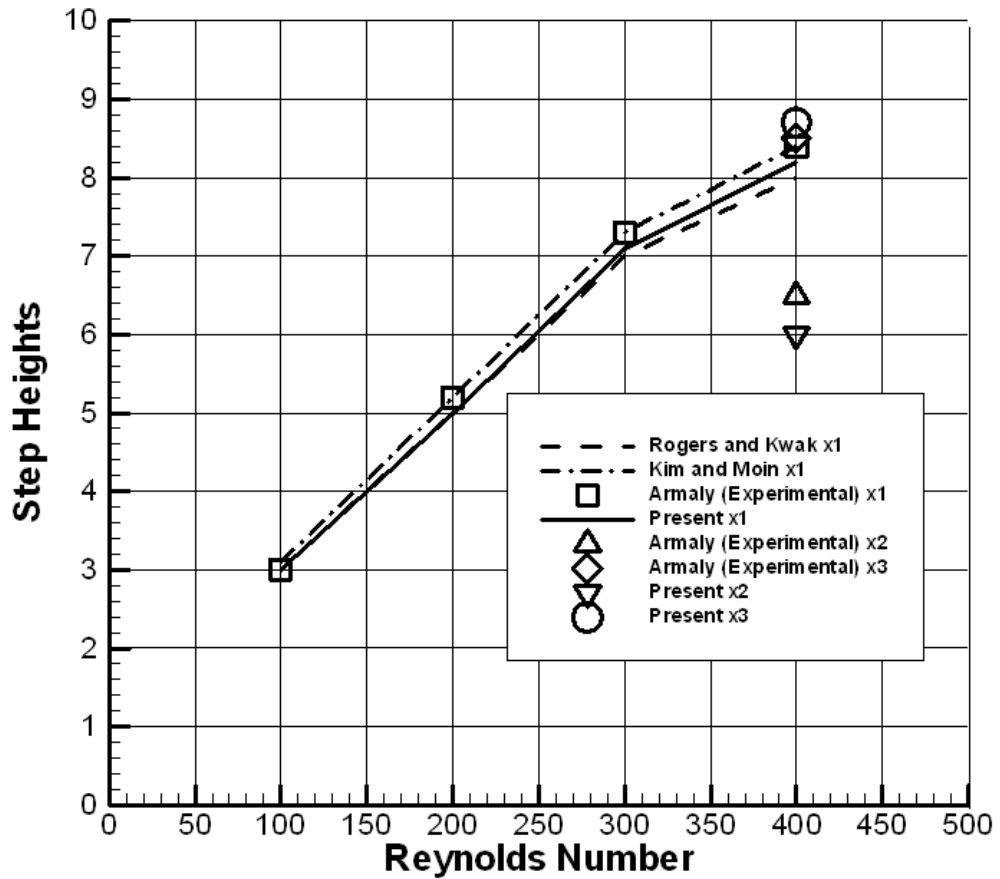


Figure 4.19: Variation of x_1, x_2 and x_3 with Reynolds Number

In figure 4.19 the quantities x_1 , x_2 and x_3 are plotted against Reynolds number for present computed result and the result reported by Rogers et. al. (1991) and experimental results of Armaly et al. (1983). Good agreement is seen between these results for the value of x_1 , at the lower Reynolds numbers before the secondary separation appears. At a Reynolds number of 400, the secondary separation bubble is present and the values of x_2 and x_3 are compared. In their experiment, Armaly et al.(1983) reported that the flow was found to be three-dimensional near the step for Reynolds number of 400 and above, and that the three-dimensional effects were negligible for lower Reynolds numbers. These three-dimensional effects could explain the discrepancies between calculation and experiment.

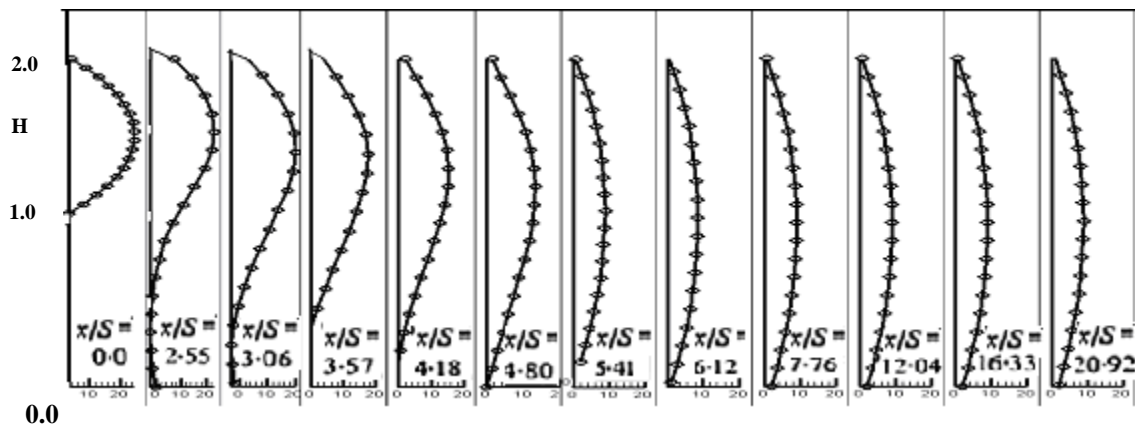
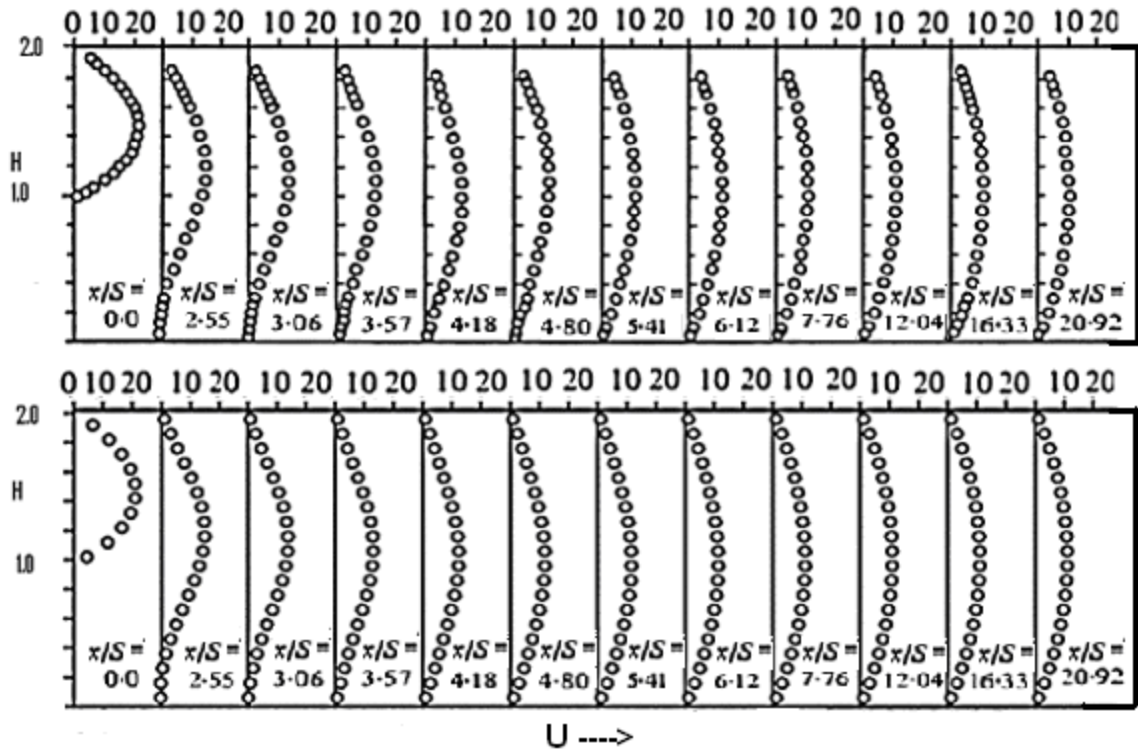


Figure 4.20 Velocity profiles at various downstream locations for backward facing step problem ($Re=100$); Top figure Armaly et.al [1983], middle figure Erturk [2008], bottom figure present study

Next we compare a set of experimental and numerical solutions found in the literature with the present computational result in order to demonstrate the accuracy of the present numerical solutions. Figure 4.20 shows the u -velocity profile at several x -locations (plotted as a fraction of the total length of the configuration S , i.e. $\frac{x}{S}$. In this plot $x=0$ is taken at the step location) at Reynolds

number $Re=100$ for the experimental results presented by Armaly et al. (1983) for a backward facing step. For the same geometry a numerical solution for a steady two-dimensional flow is also presented by Erturk (2008) and the u-velocity profiles at the corresponding x-locations drawn to the same scale is shown in the figure 4.20. Next the computed u-velocity profiles at the same x locations from the simulation with the present method are drawn for comparison. From the figure 4.20 it can be seen that the present computed velocity profiles agree well with that of experimental results of Armaley et al. (1983) and numerical result of Erturk (2008).

4.5 Laminar axisymmetric sudden expansion flow

Flows through sudden enlargements are of interest from the point of view of fundamental fluid mechanics as well as practical applications. There is keen interest in the understanding of such flows due to their widespread occurrence in many fluid applications including heat exchangers, combustors, and nuclear reactors as well as in biological systems. On the fundamental fluid mechanics side, the flow through an axisymmetric sudden expansion has all the complexities of an internally separating and reattaching flow. However, it is relatively easy to study numerically since the point of separation is fixed by the expansion step while the geometry affords a straightforward numerical scheme in the rectangular coordinates. For this reason, the laminar axisymmetric sudden expansion flow has become a standard problem to test the performance of different computational schemes. The gross features of the axisymmetric sudden expansion flow, both laminar and turbulent, are fairly well known through flow visualizations and some quantitative studies. However, the details of this flow structure such as velocity distributions, wall pressure and shear stress, redevelopment length and recirculation flow strength, are not well understood.

The turbulent axisymmetric sudden expansion flow has been investigated both experimentally and numerically by a number of researchers. The details of the flow structure, as well as the influence of inlet conditions, are fairly well understood in this flow regime. On the other hand, the number of studies

involving the laminar axisymmetric sudden expansion flow is quite limited. The literature on the experimental investigations of this flow is even more limited and quantitative results obtained in a systematic fashion covering a range of Reynolds numbers is currently lacking. For this reason, most of the previous studies of the laminar axisymmetric sudden expansion flows have essentially been limited to flow visualizations. These studies showed that the size of the recirculation region downstream of the expansion increases with increasing Reynolds numbers within the laminar flow regime.

A systematic study of the laminar sudden expansion flow was undertaken in the Reynolds number range of $Re= 20$ to 211 . The selected Reynolds numbers insured instability-free laminar flow in the complete range of study; the lowest critical Reynolds number reported in the literature for the onset of flow instabilities is $Re=300$. Hammad et. al. (1999) has done a digital PIV technique in order to provide quantitative data to form a baseline for computational studies. It was also the aim of this study to investigate effect of Reynolds number on the length of recirculation zone and other features of the flow. The results obtained from the present code have been compared with this set of experimental data. The geometry of the pipes used to run the code is shown in the figure 4.21 along with the boundary condition.

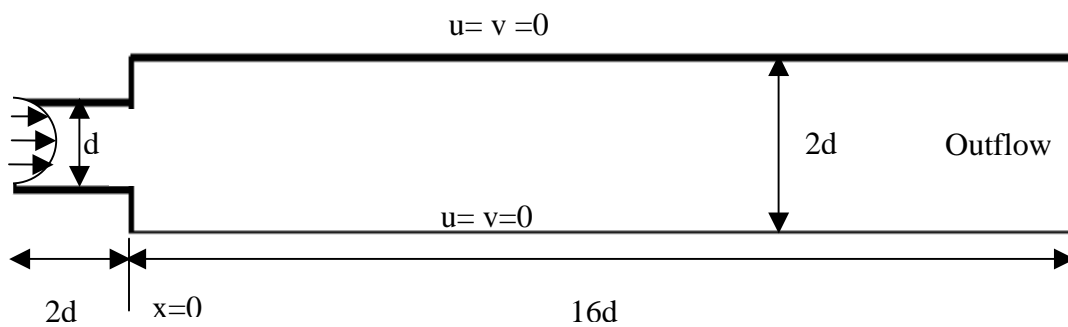
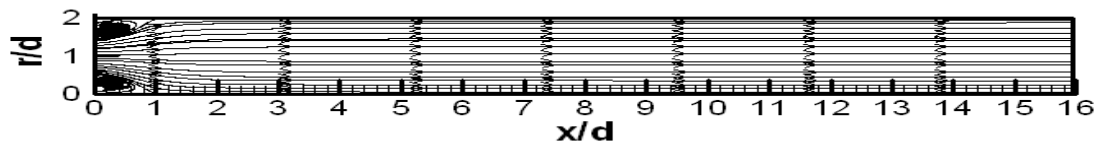
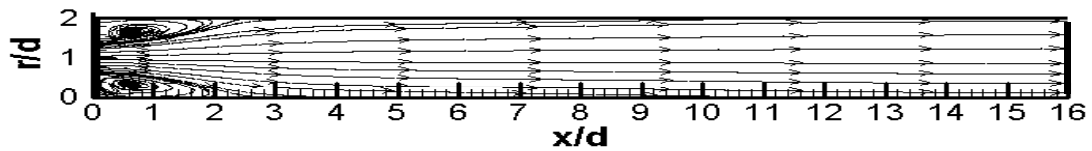


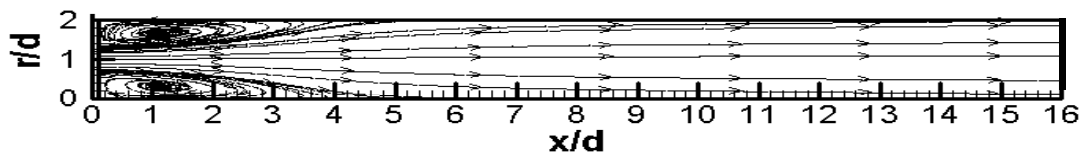
Figure 4.21: Geometry and boundary conditions used for sudden expansion flow problem



a) $Re=20.6$



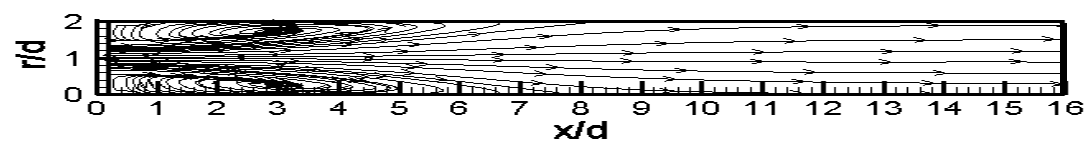
b) $Re=55.4$



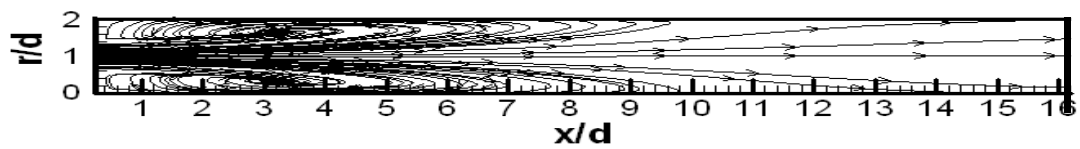
c) $Re=77.6$



d) $Re=109.0$



e) $Re=156.1$,



f) $Re=211.1$

Figure 4.22: Streamline plots for sudden expansion problem for different Reynolds number

The set of Reynolds number for which the code has been run are $Re=20.6, 55.4, 77.8, 109, 156.1$ and 211.1 . The streamline plots have been shown in the figure 4.22 for the above Reynolds number based on smaller pipe diameter. The fluid enters the expanded zone as a fully developed flow in order to ensure fully developed flow conditions upstream of the expansion. This allows for a meaningful comparison of the different Reynolds number cases. As the Reynolds number increases, the flow takes a longer axial distance to adjust to the sudden change in the pipe cross-sectional area. Also it has been observed that no flow instabilities exist even for $Re=211$ as stated by Hammad (1999). As the Reynolds number is increased the expanded flow becomes straighter and it reaches the wall at increasing axial distances from the expansion step. Furthermore, higher Reynolds numbers result in stronger flow recirculation as indicated by the existence of streamlines with progressively larger negative values.

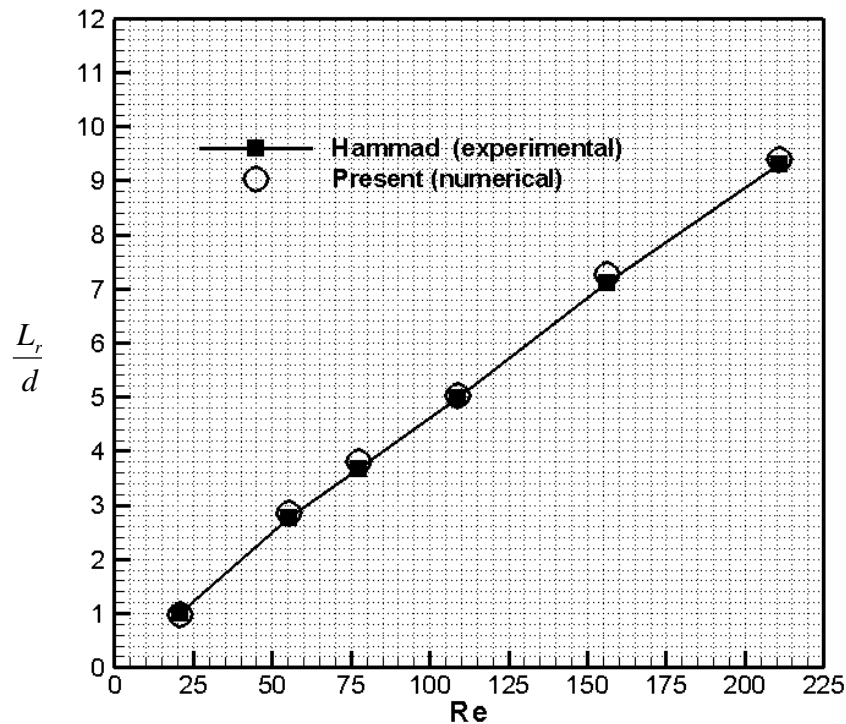


Figure 4.23: Comparison of dependence of reattachment length on Reynolds number

The reattachment length L_r , on the other hand, is a linear function of the Reynolds number as shown in figure 4.23. In this figure, the present results are compared to results reported by Hammad et. al. (1999) obtained experimentally

by PIV techniques. The agreement between those results and the present quantitative measurements is very strong confirming the earlier experimental observations that the reattachment length is roughly a linear function of the Reynolds number in this flow regime.

4.6 Condition number analysis

In the numerical analysis, the condition number associated with a problem is a measure of that problem's amenability to digital computation, that is, how numerically well-conditioned the problem is. A problem with a low condition number is said to be well-conditioned, while a problem with a high condition number is said to be ill-conditioned. For square matrices we can measure the sensitivity of the solution of the linear algebraic system

$$\mathbf{Ax} = \mathbf{b} \quad (4.11)$$

with respect to changes in vector \mathbf{b} and in matrix \mathbf{A} by using the notion of the condition number of the matrix \mathbf{A} . Condition number is defined as the product of norm of \mathbf{A} and the norm of \mathbf{A} inverse

$$\kappa = \|\mathbf{A}\| \|\mathbf{A}^{-1}\| \quad (4.12)$$

Condition number depends on the underlying norm. However, regardless of the norm, it's always greater than or equal to 1. If it's close to one, matrix is well conditioned which means it's inverse can be computed with good accuracy. If the condition number is large, when the matrix is said to be ill conditioned, and computation of it's inverse, or solution of a linear system of equations is prone to large numerical errors. The condition number associated with the linear equation (4.11) gives a bound on how inaccurate the solution \mathbf{x} will be after approximate solution. Conditioning is a property of the matrix, not the algorithm or floating point accuracy of the computer used to solve the corresponding system. The definition of condition number depends on the choice of the norm. If $\|\cdot\|$ is l_2 norm then

$$\kappa(\mathbf{A}) = \frac{\sigma_{\max}(\mathbf{A})}{\sigma_{\min}(\mathbf{A})} \quad (4.13)$$

where, $\sigma_{\max}(\mathbf{A})$ and $\sigma_{\min}(\mathbf{A})$ are maximal and minimal singular values of \mathbf{A} respectively. Therefore if \mathbf{A} is normal then

$$\kappa(\mathbf{A}) = \frac{|\lambda_{\max}(\mathbf{A})|}{|\lambda_{\min}(\mathbf{A})|} \quad (4.14)$$

where, $\lambda_{\max}(\mathbf{A})$ and $\lambda_{\min}(\mathbf{A})$ are maximum and minimum (by modulus) eigenvalues of \mathbf{A} respectively. Now substituting the values of maximum and minimum eigenvalues from equation (4.14) we get

$$\kappa(\mathbf{A}) = \frac{|u + \sqrt{u^2 + \delta}|}{|u - \sqrt{u^2 + \delta}|} \quad (4.15)$$

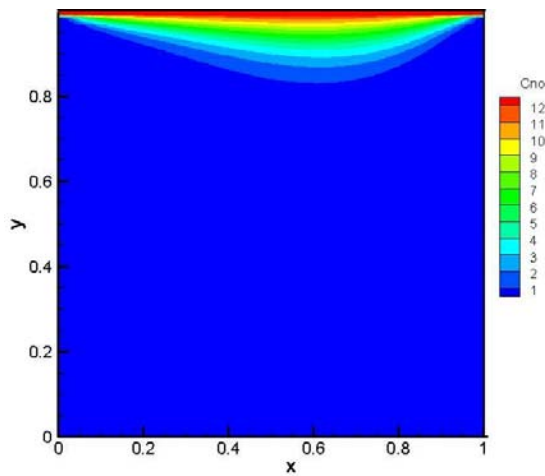
The values of condition numbers have been computed for the following four cases of

- Flow inside lid driven cavity at Reynolds number=400
- Flow past a circular cylinder at Reynolds number=40
- Flow over a backward facing step at Reynolds number=400
- Laminar axisymmetric sudden expansion flow at Reynolds number=211

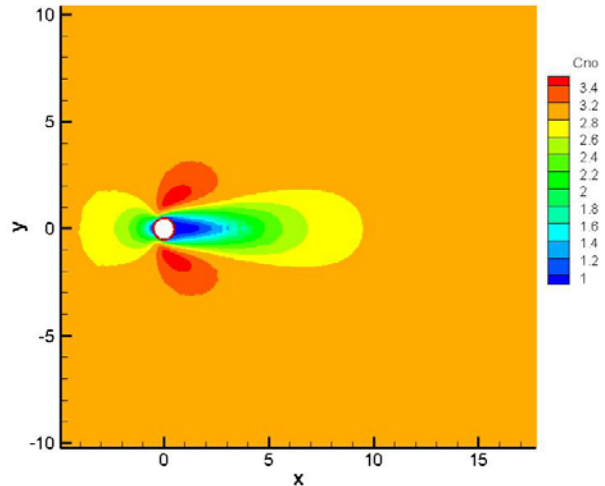
The results are shown in figure 4.24. The values of maximum and minimum condition number for the above four cases and the values of corresponding artificial compressibility parameter has been given in the following table.

Table 4.2 Values of condition number and artificial compressibility parameter

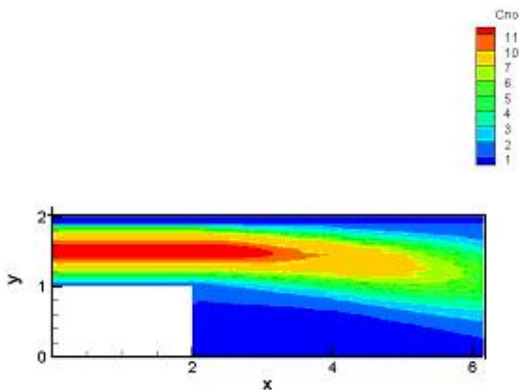
Case	δ	Max. Condition No
Lid driven cavity	1.0	12.0
Circular cylinder	1.0	3.4
Backward facing step	1.0	11.0
Sudden expansion	1.0	8.0



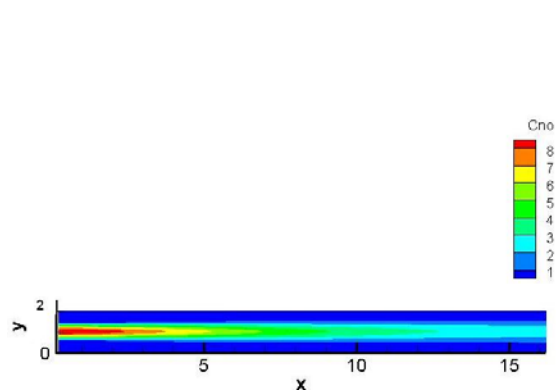
a) Flow inside lid driven cavity at Reynolds number=400



b) Flow past a circular cylinder at Reynolds number=40



c) Flow over a backward facing step at Reynolds number=400



d) Laminar axisymmetric sudden expansion flow at Reynolds number=211

Figure 4.24 Condition number contours for flow simulation using meshless ACM based solver for different geometries

It is observed that higher value of condition number occur at top moving plate of the lid driven cavity and entry region of the backward facing step. For laminar axisymmetric sudden expansion flow the maximum value of condition number obtained is 8.0 whereas for flow past a circular cylinder highest value of condition number obtained is 3.4.

4.7 Summary

In this chapter the capabilities of the present method are demonstrated by simulating the test cases of fully developed flow inside a channel, external flow

over a flat plate (Blasius Solution), flow inside a lid driven cavity, flow past a circular cylinder, flow over a backward facing step and laminar axisymmetric sudden expansion flow. Finally condition number analyses of a few selected cases have been presented.

CHAPTER 5

Conclusions and future work

5.0 Conclusion

Artificial Compressibility Method (ACM) of solution for the incompressible Navier-Stokes equations using meshless least square based discretization has been tested. A few benchmark problems have been solved to test the capability of the code. A simple flow problem between two parallel plates has been solved using this method for varying Reynolds number from 0 to 1000. It is observed that convergence is faster when Reynolds number is smaller and solution is obtained using lesser number of grid points and higher values of the artificial compressibility parameter. But as the Reynolds number increases more and more grid points are required as well as convergence becomes slower. Also value of artificial compressibility parameter δ had to be brought down. Convergence to the steady state can be further accelerated by optimizing the parameters, time step Δt and δ , to be assigned values that make convergence to the steady solution as rapid as possible. The stability condition restricts the range of permissible values of these parameters. If other types of boundary conditions are imposed, e.g., if the derivatives of the velocities are prescribed at the boundary, one has to ensure that no instabilities arise due to boundary effects. Finally, it has been observed that the accuracy of the scheme can be improved in two-dimensional problems with grid enhancement or clustering near the boundary.

Next, the external flow over a flat plate (Blasius solution) has been solved for Reynolds number of 10,000. The solution obtained is self-similar and matches well with the Blasius solution. Another widely accepted benchmark problem of incompressible flow inside a lid driven cavity for lower range of three different Reynolds numbers 100, 400 and 1000 has been solved using the ACM code

developed. The solution matches well with that provided by Ghia (1982) for these range of Reynolds numbers.

Next, the capabilities of the present method are demonstrated by simulating the laminar flow over a circular cylinder. This test case is particularly important in order to test the grid free or meshless nature of the ACM code with least square based discretization method adopted in the present work. As this method works on an arbitrary distribution of points and requires connectivity or neighbourhood information for every point in the 'cloud of points' it is extremely flexible for complex geometry and multibody configuration. Steady state solution for three different Reynolds numbers have been computed and results are compared with standard results available in the literature. The solution obtained through the ACM code developed matches well with that available in the literature.

Next the problem of flow over a backward facing step that contains rich flow features like flow separation, flow reattachment and multiple recirculating zones have been tried with the present code. All the above features are successfully captured and compare well with those available in the literature.

Finally the laminar axisymmetric sudden expansion flow problem has been solved. In the Reynolds number range covered by the study, the velocity field does not show any asymmetry on the vertical plane; the radial velocity on pipe axis is zero throughout and the top and bottom reattachment lengths are approximately the same. Higher Reynolds numbers lead to longer reattachment lengths. The reattachment lengths are linear functions of the Reynolds number. The result has been compared with the reported experimental results available in the literature and compares well.

The results of the driven cavity flow problem and the flow past a circular cylinder at low Reynolds numbers for two-dimensional steady incompressible Navier–Stokes problem further show that the least square based ACM method

can be successfully employed for simulation of the incompressible viscous flow. Hence it can be concluded that an meshless incompressible viscous two-dimensional Navier-Stokes solver using artificial compressibility method has been developed that can be applied to any irregular geometry and requires information of a 'cloud of points'.

5.1 Future Work

Further some major improvement can be worked out above the current code aimed as future work. These are

- Introduction of energy equation in the current code to solve heat transfer related problems.
- Extend the capabilities of the ACM code developed to handle transient problems.
- Extend the code into three dimensional flow regimes.
- Introduction of turbulence modeling

Appendix A

In one dimension the least square approximation to the first order accurate derivative (in x) f_{x_0} at the point o is given by

$$f_{x_0}^{(1)} = \frac{\sum \Delta x_i \Delta f_i}{\sum \Delta x_i^2} \quad (\text{A.1})$$

where $\Delta x_i = x_i - x_0$ and $\Delta f_i = f_i - f_0$ as before. Now considering the Taylor expansion

$$\Delta f_i = \Delta x_i \left(\frac{\partial f}{\partial x} \right)_o + \frac{\Delta x_i^2}{2} \left(\frac{\partial^2 f}{\partial x^2} \right)_o + H \quad (\text{A.2})$$

where H =higher order terms. Now we note

$$\Delta f_{x_i} = \Delta x_i \left(\frac{\partial f}{\partial x} \right)_o + H \quad (\text{A.3})$$

This suggests that Δf_{x_i} can be used to cancel the second derivative term in equation (A.2). Now we can define a modified difference as

$$\Delta \tilde{f}_i = \Delta f_i - \frac{\Delta x_i}{2} \Delta f_{x_i}^{(1)} \quad (\text{A.4})$$

where,

$$\Delta f_{x_i}^{(1)} = f_{x_i}^{(1)} - f_{x_0}^{(1)} \quad (\text{A.5})$$

The difference $\Delta f_{x_i}^{(1)}$ can be calculated by using the first order formula (A.1) and it can then be used to determine the modified difference $\Delta \tilde{f}_i$ using equation (A.4).

From equation (A.2) and (A.4) we get

$$\Delta \tilde{f}_i = \Delta x_i \left(\frac{\partial f}{\partial x} \right)_o + O(\Delta x_i^3) \quad (\text{A.6})$$

Hence the second -order accurate formula for f_{x_0} is given by

$$f_{x_0}^{(2)} = \frac{\sum \Delta x_i \Delta \tilde{f}_i}{\sum \Delta x_i^2} \quad (\text{A.7})$$

Thus we get a two-step second order accurate formula to calculate $f_{x_0}^{(2)}$. In the first step first order accurate $f_{x_0}^{(1)}$ and the modified difference $\Delta\tilde{f}_i$ is determined. In the second step using equation (A.7) the second order accurate $f_{x_0}^{(2)}$ is calculated.

The above two-step formula can easily be extended to a two dimensional problem. Here in the first step as described above the first order accurate derivatives $f_{x_0}^{(1)}, f_{y_0}^{(1)}$ are calculated as following (without the weight factors)

$$\begin{aligned} f_{x_0}^{(1)} &= \frac{\sum \Delta y_i^2 \sum \Delta x_i \Delta f_i - \sum \Delta x_i \Delta y_i \sum \Delta y_i \Delta f_i}{\sum \Delta x_i^2 \sum \Delta y_i^2 - (\sum \Delta x_i \Delta y_i)^2} \\ f_{y_0}^{(1)} &= \frac{\sum \Delta x_i^2 \sum \Delta y_i \Delta f_i - \sum \Delta x_i \Delta y_i \sum \Delta x_i \Delta f_i}{\sum \Delta x_i^2 \sum \Delta y_i^2 - (\sum \Delta x_i \Delta y_i)^2} \end{aligned} \quad (A.8)$$

Then the modified differences can be calculated as

$$\Delta\tilde{f}_i = \Delta f_i - \frac{\Delta x_i}{2} \Delta f_{x_i}^{(1)} - \frac{\Delta y_i}{2} \Delta f_{y_i}^{(1)} \quad (A.9)$$

$$\Delta f_{x_i}^{(1)} = f_{x_i}^{(1)} - f_{x_0}^{(1)}, \quad \Delta f_{y_i}^{(1)} = f_{y_i}^{(1)} - f_{y_0}^{(1)} \quad (A.10)$$

In the second step the second-order accurate derivatives $f_{x_0}^{(2)}, f_{y_0}^{(2)}$ can be calculated as following

$$\begin{aligned} f_{x_0}^{(2)} &= \frac{\sum \Delta y_i^2 \sum \Delta x_i \Delta\tilde{f}_i - \sum \Delta x_i \Delta y_i \sum \Delta y_i \Delta\tilde{f}_i}{\sum \Delta x_i^2 \sum \Delta y_i^2 - (\sum \Delta x_i \Delta y_i)^2} \\ f_{y_0}^{(2)} &= \frac{\sum \Delta x_i^2 \sum \Delta y_i \Delta\tilde{f}_i - \sum \Delta x_i \Delta y_i \sum \Delta x_i \Delta\tilde{f}_i}{\sum \Delta x_i^2 \sum \Delta y_i^2 - (\sum \Delta x_i \Delta y_i)^2} \end{aligned} \quad (A.11)$$

Hence it can be observed that in the above two-step formulae the first-order formulae has been repeatedly used and it has been found to be very robust, Deshpande (1998).

Appendix B

The present method like Lattice Boltzmann method is also based on the kinetic theory of gases. The crucial feature in both the method is the equilibrium distribution function, which describes the velocity distribution of the particles / molecules of liquid at thermal equilibrium in terms of the macroscopic state variables following the approach of Junk et al. (1999).

In order to understand the behavior of kinetic scheme in the incompressible limit (i.e. when $u \ll$ speed of sound) we need to choose time scale $\varsigma = \frac{L}{U}$, where U is the typical speed and L is the length scale of the flow.

Density is assumed to be of the order unity. Then the governing equations are

$$\frac{\partial \rho}{\partial t} + \text{div}(\rho \mathbf{u}) = 0 \quad (\text{B1})$$

$$\frac{\partial(\rho \mathbf{u})}{\partial t} + \text{div}(\rho \mathbf{u} \otimes \mathbf{u} + c_s^2 \rho \mathbf{I}) = \text{div}(\boldsymbol{\eta}) \quad (\text{B2})$$

where

c_s = speed of sound , and

viscous stress tensor is given by

$$\boldsymbol{\eta} = \nu \rho (2\mathbf{S} + \text{div} \mathbf{u}) \mathbf{I},$$

$$S_{ij} = \frac{1}{2} \left(\frac{\partial u_i}{\partial x_j} + \frac{\partial u_j}{\partial x_i} \right)$$

after scaling the above equations (B1-B2) become

$$\frac{\partial \rho}{\partial t} + \varsigma \frac{U}{L} \text{div}(\rho \mathbf{u}) = 0 \quad (\text{B3})$$

$$\frac{\partial(\rho \mathbf{u})}{\partial t} + \varsigma \frac{U}{L} \text{div}(\rho \mathbf{u} \otimes \mathbf{u}) + c_s^2 \frac{\varsigma}{LU} \rho \mathbf{I} = \frac{\varsigma}{L^2} \text{div} \boldsymbol{\eta} \quad (\text{B4})$$

now by assumption

$$\frac{c_s U}{L} = 1 \text{ and } \frac{c_s^2 \zeta}{LU} = \frac{c_s^2}{U^2}$$

Introducing $Ma = \frac{U}{c_s}$ and Reynolds number $Re = \frac{UL}{\nu}$ for the flow and making use

of we equation (B1) finally we get

$$\frac{\partial(\rho u)}{\partial t} + \text{div}(\rho u \otimes u) + \frac{1}{Ma^2} \nabla \rho = \frac{1}{Re} \text{div}(2\rho S + \rho \text{div} u) \quad (B5)$$

For any explicit compressible flow solver to work in incompressible limit has to get a reasonable space resolution. For this time resolution must be extremely fine (if $Ma \ll 1$) to satisfy the CFL condition. Consistency analysis carried out in the coupled limit

$$\begin{aligned} \Delta t &\rightarrow 0 \\ Ma &\rightarrow 0 \end{aligned} \quad (B6)$$

assuming

$$\frac{\Delta t}{Ma^2} = \zeta = \text{constant} \quad (B7)$$

Junk et al (1999) have further assumed

$$\rho = \bar{\rho}(1 + Ma^2 p) \quad (B8)$$

and observed

$$Ma^2 = O(\Delta t) \quad (B9)$$

leading to

$$\text{div}(u) = O(\Delta t) \quad (B10)$$

The structure of ρ reduces the Navier stokes equation order error term

$$\frac{\partial u}{\partial t} + (u \cdot \nabla) u + \nabla p = \left(\frac{1}{Re} + \frac{1}{2} \zeta \right) \Delta u + O(\Delta t) \quad (B11)$$

Leading to

$$\frac{\partial p}{\partial t} + (u \cdot \nabla) p + \frac{1}{Ma^2} \text{div} u = \frac{1}{2} \zeta \Delta p + \text{div}((u \cdot \nabla) u) + O(\Delta t) \quad (B12)$$

Equation of this type is similar to the equation used in pseudo-compressibility method to ensure divergence free condition. This can be cast in the following form of Chorin's Artificial Compressibility Method (reference equation 2.8)

$$\frac{1}{\delta} \frac{\partial p}{\partial t} + \text{div} u = 0 \quad (\text{B13})$$

Junk et. al. (1999) have concluded that in the

“In the coupled limit $\Delta t, Ma \rightarrow 0$ with $\frac{\Delta t}{Ma^2} = \zeta$ with the assumption that $\rho = \bar{\rho}(1 + Ma^2 p)$ and that u, p and their derivatives are order one functions, the Kinetic Scheme is consistent to the incompressible Navier Stokes equation with effective Reynolds number “

$$\frac{1}{\text{Re}'} = \frac{1}{\text{Re}} + \frac{\lambda}{2} \quad (\text{B14})$$

and density is replaced by artificial equation of state

$$p = \rho \delta \quad (\text{B15})$$

where ρ is an artificial density, equated to the product of inverse of artificial compressibility factor δ and pressure p by the artificial equation of state. Here,

$\frac{\partial \rho}{\partial \tau} \rightarrow 0$ at the steady state and τ is a fictitious time. Since this is an artificial equation of state, then $\delta^{1/2}$ plays the role of an artificial sound speed. Here it is important to note that at steady state the solution is independent of ρ and τ .

Governing Equations of ACM in Flux Form

Reference equation (2.33)

$$\frac{\partial}{\partial \tau} (\mathbf{U}) + \frac{\partial}{\partial x} (\mathbf{GX}_I + \mathbf{GX}_V) + \frac{\partial}{\partial y} (\mathbf{GY}_I + \mathbf{GY}_V) = 0 \quad (\text{B16})$$

Where

$$\mathbf{U} = \begin{bmatrix} p \\ u \\ v \end{bmatrix}, \quad \mathbf{GX}_I = \begin{bmatrix} \delta u \\ u^2 \\ uv \end{bmatrix}, \quad \mathbf{GY}_I = \begin{bmatrix} \delta v \\ uv \\ v^2 \end{bmatrix}, \quad \mathbf{GX}_V = \begin{bmatrix} 0 \\ \tau_{xx} + p \\ \tau_{xy} \end{bmatrix}, \quad \mathbf{GY}_V = \begin{bmatrix} 0 \\ \tau_{yx} \\ \tau_{yy} + p \end{bmatrix}$$

Expressions for the 2-D inviscid fluxes

The expression of x-component of the inviscid split-flux is given by

$$\begin{aligned}
 GX_i^\pm(1) &= \frac{\delta}{\sqrt{\beta}} \left\{ s_1 A_i^\pm \pm \frac{B_1}{\sqrt{\pi}} \right\} \\
 GX_i^\pm(2) &= \frac{1}{\beta} \left\{ s_1^2 A_i^\pm \pm \frac{B_1}{\sqrt{\pi}} s_1 \right\} \\
 GX_i^\pm(3) &= \frac{1}{\beta} s_2 \left\{ s_1 A_i^\pm \pm \frac{B_1}{\sqrt{\pi}} \right\}
 \end{aligned} \tag{B17}$$

The expression of y-component of the inviscid split-flux is given by

$$\begin{aligned}
 GY_i^\pm(1) &= \frac{\delta}{\sqrt{\beta}} \left\{ s_2 A_i^\pm \pm \frac{B_2}{\sqrt{\pi}} \right\} \\
 GY_i^\pm(2) &= \frac{1}{\beta} s_1 \left\{ s_2 A_i^\pm \pm \frac{B_2}{\sqrt{\pi}} \right\} \\
 GX_i^\pm(3) &= \frac{1}{\beta} \left\{ s_2^2 A_i^\pm \pm \frac{B_2}{\sqrt{\pi}} s_2 \right\}
 \end{aligned} \tag{B18}$$

where,

δ = Artificial compressibility parameter

$$\beta = \frac{1}{2\delta}$$

$$B_i = \frac{e^{-s_i^2}}{2}$$

$$A_i^\pm = \frac{1 \pm \text{erf}(s_i)}{2}$$

$$s_i = u_i \sqrt{\beta}$$

The artificial equation of state given by equation (B15)

$$p = \rho \delta$$

At incompressible limit the transient term in equation (B16) vanishes.

References

- Agarwal, L., “Computations of incompressible flow with an application to moderator flow”, Ph.D. Thesis, Indian Institute of Technology, Mumbai, 2001.
- Armaly, B.F., Durst, F., Periera, J.C.F., Schonung, B., “Experimental and theoretical investigation of backward-facing step flow”, *Journal of Fluid Mechanics*, 127, pp. 473-481, 1983.
- Atluri, S.N., Lin, H., “The meshless local Petrov–Galerkin (MLPG) method for solving incompressible Navier–Stokes equations”, *CMES: Comp. Modeling Eng. Sci.* 2 (2), pp. 117-142, 2001.
- Atluri, S.N., Shen, S., “The meshless local Petrov-Galerkin (MLPG) method”, Tech Science Press, 2002.
- Atluri, S.N., Zhu, T.L., “The meshless local Petrov-Galerkin (MLPG) approach for solving problems in elasto-statics”, *Computational Mechanics*, 25, pp. 169-179, 2000.
- Balakrishnan, N., “New least squares based finite difference methods”, Report No. 99-FM9, Department of Aerospace Engineering, IISc, Bangalore, 1999.
- Balakrishnan, N., Praveen, C., “A new upwind least squares finite difference scheme (LSFD-U) for Euler equations of gas dynamics,” *Finite Volume for Complex Applications – II*, Hermes Science, Paris, pp. 269-281, 1999.

- Balakrishnan, N., Sridar, D., “On a generalised finite difference framework and its order of accuracy”, Satofuka, N., (Ed.), Proceedings of Computational Fluid Dynamics 2000, Springer, Berlin, 2000.
- Barton, I.E., “Improved laminar predictions using a stabilized time dependant simple scheme”, International Journal for Numerical Methods in Fluids, 28, pp 841-857, 1998.
- Batina, T.J. “A gridless Euler / Navier–Stokes solution algorithm for complex aircraft applications”, AIAA Paper No. 93-0333, 1993.
- Beam, R.M., Warming, R.F., “An implicit finite-difference algorithm for hyperbolic systems in conservation-law form (application to Eulerian gas dynamic equations)”, Journal of Computational Physics, 22, pp. 87-110, 1976.
- Belytschko, T., Krongauz, Y., Organ, D., Fleming, M., Krysl P., “Meshless methods: An overview and recent developments”. Computer Methods in Applied Mechanics and Engineering. 139, pp. 3-47,1996.
- Benjamin, A.S., Denny, V.E., “On the convergence of numerical solutions for 2-D flows in a cavity at large Re”, Journal of Computational Physics, 33, pp. 340-358, 1979.
- Chang, J.L.C., Kwak, D., Rogers, S.E., Yang, R.L., “Numerical simulation methods of incompressible flows and an application to the space shuttle main engine”, International Journal for Numerical Methods in Fluid, 8, pp. 1241-1266, 1988.
- Choi, D., Merkle, C.L., “Application of time-iterative scheme to incompressible flow”, AIAA Journal, 23(10), pp. 1518-1524, 1985.

- Choi, Y.H., Merkle, C.L., “The application of preconditioning in viscous flows”, *Journal of Computational Physics*, 105, pp. 207-223, 1993.
- Chorin, A.J., “A numerical method for solving incompressible viscous flow problems”, *Journal of Computational Physics*, 2, pp.12-26, 1967.
- Chorin, A.J., “Numerical solution of the Navier-Stokes equations”, *Mathematics and Computers*, 22, pp. 742-762, 1968.
- Chung, K.C., “A generalised finite difference method for heat transfer problems of irregular geometries”, *Numerical Heat Transfer*, 4, pp. 345–357, 1981.
- Chung, T.J., *Computational Fluid Dynamics*, Cambridge University Press, pp. 108-110, 2002.
- Dennis, S.C.R., Chang, G.Z., “Numerical solutions for steady flow past a circular cylinder at Reynolds number up to 100”, *Journal of Fluid Mechanics*, 42(3), pp. 471-489, 1970.
- Deshpande, S.M., Ghosh, A.K., Mandal, J.C. “Least squares weak upwind methods for Euler equations”, Report No. 89-FM9, Department of Aerospace Engineering, IISc, Bangalore, 1989.
- Deshpande, S.M., Kulkarni P.S., Ghosh A.K., “New developments in kinetic schemes”, *Computers and Mathematics with Applications*, 35(1,2), pp. 75-93, 1998.
- Dick, E., “A flux-vector splitting method for steady Navier-Stokes equation”, *International Journal for Numerical Methods in Fluid*, 8, pp. 1217-1227, 1988.

- Ding, H., Shu, C., Yeo, K.S., Xu, D., "Simulation of incompressible viscous flows past a circular cylinder by hybrid FD scheme and meshless least square-based finite difference method", *Computer Methods in Applied Mechanics and Engineering*, 193, pp. 727-744, 2004.
- Duarte, C.A., Oden, J.T., "An h - p adaptive method using clouds", *Computer Methods in Applied Mechanics and Engineering*, 39 (1-4), pp. 237-262, 1996.
- Erturk, E., "Numerical solutions of 2-D steady incompressible flow over a backward-facing step, Part I: High Reynolds number solutions", *Computers and Fluids*, 37, pp. 633-655, 2008.
- Fornberg, B., "A numerical study of steady viscous flow past a circular cylinder", *Journal of Fluid Mechanics*, 98, pp. 819-855, 1980.
- Gartling, D.K., "A test problem for outflow boundary condition-flow over a backward-facing step", *International Journal of Numerical Methods in Fluids*, 11, pp 953-967, 1990.
- Ghia, U., Ghia, K.N., Shin C.T., "High-Re solutions for incompressible flow using the Navier-Stokes equations and multigrid method", *Journal of Computational Physics*, 48, pp. 387-411, 1982.
- Ghosh, A.K., "Robust least squares kinetic upwind method for inviscid compressible flows", Ph.D. Thesis, Department of Aerospace Engineering, IISc, Bangalore, 1996.
- Gingold, R.A., Monaghan, J.J., "Smoothed particle hydrodynamics: theory and application to nonspherical stars", *Monthly Notices of the Royal Astronomical Society*, 181, pp. 275-389, 1977.

- Gorski, J.J., “Incompressible cascade calculation using an upwind differential TVD scheme”, *Advances and Application in Computational Fluid Dynamics*, Baysal, O., (Ed.), pp. 61-69, 1988.
- Gorski, J.J., “TVD solution of the incompressible Navier-Stokes equation with an implicit multigrid scheme”, *AIAA Paper No. 88- 3699*, 1988.
- Guj, G., Stella, F., “Numerical solutions of high-Re recirculating flows in vorticity-velocity form”, *International Journal for Numerical Methods in Fluids*, 8, pp. 405-416, 1988.
- Hakimi, N., “Preconditioning methods for time dependent Navier Stokes equation”, Ph. D Thesis, Department of Fluid Mechanics, Vrije University, Brussels, 1997.
- Hammad, K.J., Otugen, M.V., Arik, E.B., “A PIV study of the laminar axisymmetric sudden expansion flow”, *Experiments in Fluids*, 26, pp. 266-272, 1999.
- Harlow, F.H. "The particle-in-cell computing method for fluid dynamics", *Methods for Computational Physics*, 3, pp. 319–343, 1964.
- Hirsch, C., Hakimi, N., “Preconditioning methods for time marching Navier Stokes solvers”, *Solution techniques for large scale CFD problems*, Habashi, W.G., (Ed.), Wiley, New York, pp. 334-353, 1995.
- Junk, M., Raghurama R.S.V., “A new discrete velocity method for Navier–Stokes equations”, *Journal of Computational Physics*, 155, pp. 178–198, 1999.

- Keskar, J., Lyn D.A., “Computations of a laminar backward-facing step flow at $Re=800$ with a spectral domain decomposition method”, *International Journal for Numerical Methods in Fluids*, 29, pp. 411-427, 1999.
- Kim, J., Moin P, “Application of a fractional-step method to incompressible Navier-Stokes equation”, *Journal of Computational Physics*, 12, pp. 308-323, 1985.
- Kim, W.W., Menon, S., “An unsteady incompressible Navier-Stokes solver for large eddy simulation”, *International Journal for Numerical Methods in Fluids*, 31, pp. 983-1017, 1999.
- Koshizuka, S., Oka, Y., “Moving particle semi-implicit method for fragmentation of incompressible fluid,” *Nuclear Science and Engineering*, 123, pp. 421–434, 1996.
- Koshizuka, S., Oka, Y., “Application of moving particle semi-implicit method to nuclear reactor safety,” *Computational Fluid Dynamics Journal*, Vol 9, pp. 366–375, 2001.
- Kwak, D., Chang, J.L.C., Shanks, S.P., Chakravarthy, S. “A three-dimensional incompressible Navier-Stokes flow solver using primitive variables”, *AIAA Journal*, 24(3), pp. 390-396, 1986.
- Kwak, D., Kiris C., Chang, S.K., “Computational challenges of viscous incompressible Flows”, *Computers and Fluids*, 34, pp. 283-299, 2005.
- Liu, W.K., Jun, S., Zhang, Y.F., “Reproducing kernel particle methods”, *International Journal for Numerical Methods in Fluids*, 20, pp. 1081–1106, 1995.

- Liu, G.R., “Mesh free methods- moving beyond the finite element method”, CRC Press, 2003.
- Liu, G.R., Gu, Y.T., “A point interpolation method for two-dimensional solids”, International Journal for Numerical Methods in Engineering, 50(4), pp. 937-951, 2001.
- Liszka, T., Orkisz, J., “The finite difference method at arbitrary irregular grids and its application in applied mechanics”, Computers & Structures, 11, pp.83– 95, 1980.
- Lohner, R., Sacco, C., Onate, E., Idelsohn, S., “A finite point method for compressible flow”, International Journal for Numerical Methods in Engineering, 53, pp. 1765–1779, 2002.
- Lucy, L.B., "A numerical approach to the testing of the fission hypothesis", Astronomy Journal, 82, pp.1013-1020, 1977.
- MacCormack, R.W., “A perspective on a quarter century of CFD research”, AIAA Paper No. 93-3291-CP, 1993.
- McHugh, P.R., Ramshaw, J.D., “Damped artificial compressibility iteration scheme for implicit calculations of unsteady incompressible flow”, International Journal for Numerical Methods in Fluid, 21, pp.141-153, 1995.
- Madsen, P.A., Schaffer H.A., “A discussion on artificial compressibility”, Coastal Engineering, 53, pp. 93-98, 2006.
- Mahendra, A.K., “Application of least squares kinetic upwind method to strongly rotating viscous flows”, M.Sc. Thesis, IISc, Bangalore, 2003.

- Mandal, J.C., Deshpande, S.M. “Kinetic flux vector splitting for Euler equations”, *Computers and Fluids*, 23 (2), pp. 447–478, 1994.
- Marx, Y.P., “Time integration schemes for the unsteady incompressible Navier-Stokes equations”, *Journal of Computational Physics*, 112, 182,1994.
- Merkle, C.L., Athavale, M., “A time accurate unsteady incompressible algorithm based on artificial compressibility’, *AIAA Paper No. 87-1137*, 1987.
- Monaghan, J.J., “An introduction to SPH”, *Computer Physics Communications*, 48, pp. 88–96, 1988.
- Morinishi, K. “An implicit gridless type solver for the Navier–Stokes equations”, *Computational Fluid Dynamics Journal*, 9 (1), pp. 21-35,2000.
- Morinishi, K. “Effective accuracy and conservation consistency of gridless type solver”, Satofuka, N., (Ed.), *Computational Fluid Dynamics 2000*, Springer, Berlin, 2000.
- Nayroles, B., Touzot, G., Villon, P. “Generalizing the finite element method: diffuse approximation and diffuse elements”, *Computational Mechanics*, 10, pp. 301-318, 1992.
- Nithiarasu, P., “An efficient artificial compressibility (AC) scheme based on the characteristic based split (CBS) method for incompressible flows” *International Journal for Numerical Methods in Engineering*, 56, pp. 1815-45,2003.

- Papanastasiou, T.C., Malamataris N., Ellwood K., “A new outflow boundary condition”, *International Journal for Numerical Methods in Fluids*,14, pp. 587-608, 1992.
- Rahman, M.M., Sikoken, T., “An artificial compressibility method for incompressible flows”, *Numerical Heat Transfer*, 40(5), pp. 391-405,2007.
- Ramesh, V., “Least squares grid-free kinetic upwind method”, Ph.D. Thesis, Department of Aerospace Engineering, IISc, Bangalore, 2001.
- Ramshaw, J.D., Mousseau, V.A., “Accelerated artificial compressibility method for steady state incompressible flow calculation”, *Computers & Fluids*, 18(4), pp. 361-367,1990.
- Rizzi, A., Erikson, L., “Computation of inviscid incompressible flow with rotation”, *Journal of Fluid Mechanics*, 153, pp. 275-312, 1985.
- Roe, P.L., “Approximate Riemann solver, parameter vectors and difference schemes”, *Journal of Computational Physics*, 43, pp. 357–372, 1981.
- Rogers, S.E., Kwak D., Kaul U.K., “On the accuracy of the pseudocompressibility method in solving the incompressible Navier-Stokes equations”, *Journal of Applied Mathematical Modeling*, 11, pp. 35-44,1987.
- Rogers, S.E., Kwak D., “An upwind differencing scheme for the steady state incompressible Navier-Stokes equations”, *Journal of Applied Numerical Mathematics*, 8, pp. 43-64,1991.

- Rogers, S. E., Kwak, D., Kiris, C., “Numerical solution of the incompressible Navier-Stokes equations for steady and time-dependent problems”, AIAA Journal, 29(4), pp. 603-610, 1991.
- Rogers, S.E., Kwak, D., Kiris C, “Upwind differencing scheme for the time accurate incompressible Navier-Stokes equations” AIAA Journal, 28, pp. 253-262, 1990.
- Rogers, S.E., Kwak D., “Steady and unsteady solution of incompressible Navier-Stokes equations”, AIAA Journal, 29, pp. 603-610,1991.
- Rosenfeld, M., Kwak, D., “A fractional step solution method for unsteady incompressible Navier-Stokes equation in generalized co-ordinate systems”, International Journal for Numerical Methods in Fluids, 13(10), pp.1311-1328, 1991.
- Schreiber, R., Keller H.B., “Driven cavity flows by efficient numerical techniques”, Journal of Computational Physics, 49, pp.310-333, 1983.
- Soh, W.Y. and Goodrich, J.W., “Unsteady solution of incompressible Navier-Stokes equations”, Journal of Computational Physics, 79, pp. 113-134,1988.
- Sridar, D., Balakrishnan N., “An upwind finite difference scheme for meshless solvers”, CFD Centre, Department of Aerospace Engineering, IISc Bangalore, 2003.
- Steger, A.K., Kutler, P., “Implicit finite-difference procedures for the computation of vortex wakes”, AIAA Journal, 15(4), pp.581-590, 1977.

- Sulsky, D., Chen, Z., Schreyer, H.L. "A particle method for history-dependent materials", *Computer Methods in Applied Mechanics and Engineering*, 118, pp.179-196, 1994.
- Takami, H., Keller, H.B., "Steady two-dimensional viscous flow of an incompressible fluid past a circular cylinder", *Physics of Fluids*, 12 (Suppl. II), pp. 11-51, 1969.
- Tanaka, N, "Development of a highly accurate interpolation method for mesh-free flow simulation I. Integration of gridless, particle and CIP methods", *International Journal for Numerical Methods in Fluids*, 30,pp. 957–976, 1999.
- Tuann, S.Y., Olson M.D., "Numerical studies of the flow around a circular cylinder by a finite element method", *Computers and fluids*, 6, pp. 219-231, 1978.
- Turkel, E., "Preconditioned methods for solving the incompressible low speed compressible equations", *Journal of Computational Physics*, 72, pp 277-298,1987.
- Turkel, E., "Preconditioning techniques in computational fluid dynamics", *Annual Review of Fluid Mechanics*, 31, pp. 567-633, 1999.
- Vanka, S. P., "Block-implicit multigrid solution of Navier-Stokes equations in primitive variables", *Journal of Computational Physics*, 65, pp. 138-158, 1986.

- Vanleer, B., Lee, W.T., Roe, P.L., “Characteristics time-stepping or local preconditioning of the Euler equations”, AIAA Paper No. 91-1552-CP, 1991.
- Vanleer, B., “Flux vector splitting for Euler equations, Lecture Notes in Physics”, 170, Springer, Berlin, 1982.
- Yagawa, G., “Seamless and parallel computing by using free mesh method: A kind of meshless technique”, Advances in meshfree and X-FEM Methods, world scientific, pp. 3-17, 2002.
- Yee, H.C., Turezyski J.R., Mortan, S.A., Visbal M.R., “On spurious behavior of CFD simulations”, International Journal for Numerical Methods in Fluids, 30, pp. 675-711, 1999.
- Yuan, S.W., “Foundations of fluid mechanics”, Prentice Hall of India, pp 312-316, 1969.
- Zhang, X.K., Kwon, K., Youn, S., “The least-squares meshfree method for the steady incompressible viscous flow”, Journal of Computational Physics, 206, pp 182–207, 2005.